NeuroImage 189 (2019) 631–644

Contents lists available at ScienceDirect

NeuroImage

journal homepage: www.elsevier.com/locate/neuroimage

The spectral exponent of the resting EEG indexes the presence of consciousness during unresponsiveness induced by propofol, xenon, and ketamine

Michele Angelo Colombo [a,*], Martino Napolitani [b,c], Melanie Boly [d], Olivia Gosseries [e], Silvia Casarotto [b], Mario Rosanova [b,f], Jean-Francois Brichant [g], Pierre Boveroux [g], Steffen Rex [h], Steven Laureys [e], Marcello Massimini [b,i], Arturo Chieregato [a], Simone Sarasso [b,**]

[a] Neurosurgical Intensive Care, ASST Grande Ospedale Metropolitano Niguarda, Milan, 20162, Italy
[b] Dipartimento di Scienze Biomediche e Cliniche "L. Sacco", Università Degli Studi di Milano, 20157 Milan, Italy
[c] Department of Health Science, School of Medicine and Surgery, University of Milan-Bicocca, Monza, Italy
[d] Department of Neurology and Department of Psychiatry, University of Wisconsin, Madison, USA
[e] Coma Science Group, GIGA-Consciousness, University and University Hospital of Liège, 4000 Liège, Belgium
[f] Fondazione Europea per La Ricerca Biomedica, Milan, Italy
[g] Department of Anaesthesia and Intensive Care Medicine, Liège University Hospital, 4000 Liège, Belgium
[h] Department of Anaesthesiology and Department of Cardiovascular Sciences, University Hospitals of the KU Leuven, KU Leuven, 3000 Leuven, Belgium
[i] Istituto Di Ricovero e Cura a Carattere Scientifico, Fondazione Don Carlo Gnocchi, 20148 Milan, Italy

ARTICLE INFO

Keywords:
EEG
Anesthesia
1/F
NCC
E/I
Consciousness

ABSTRACT

Despite the absence of responsiveness during anesthesia, conscious experience may persist. However, reliable, easily acquirable and interpretable neurophysiological markers of the presence of consciousness in unresponsive states are still missing. A promising marker is based on the decay-rate of the power spectral density (PSD) of the resting EEG.

We acquired resting electroencephalogram (EEG) in three groups of healthy participants (n = 5 each), before and during anesthesia induced by either xenon, propofol or ketamine. Dosage of each anesthetic agent was tailored to yield unresponsiveness (Ramsay score = 6). Delayed subjective reports assessed whether conscious experience was present ('Conscious report') or absent/inaccessible to recall ('No Report'). We estimated the decay of the PSD of the resting EEG—after removing oscillatory peaks—via the spectral exponent β, for a broad band (1–40 Hz) and narrower sub-bands (1–20 Hz, 20–40 Hz). Within-subject anesthetic changes in β were assessed. Furthermore, based on β, 'Conscious report' states were discriminated against 'no report' states. Finally, we evaluated the correlation of the resting spectral exponent with a recently proposed index of consciousness, the Perturbational Complexity Index (PCI), derived from a previous TMS-EEG study.

The spectral exponent of the resting EEG discriminated states in which consciousness was present (wakefulness, ketamine) from states where consciousness was reduced or abolished (xenon, propofol). Loss of consciousness substantially decreased the (negative) broad-band spectral exponent in each subject undergoing xenon or propofol anesthesia—indexing an overall steeper PSD decay. Conversely, ketamine displayed an overall PSD decay similar to that of wakefulness—consistent with the preservation of consciousness—yet it showed a flattening of the decay in the high-frequencies (20–40 Hz)—consistent with its specific mechanism of action. The spectral exponent was highly correlated to PCI, corroborating its interpretation as a marker of the presence of consciousness. A steeper PSD of the resting EEG reliably indexed unconsciousness in anesthesia, beyond sheer unresponsiveness.

* Corresponding author.
** Corresponding author.
E-mail addresses: milecombo@gmail.com (M.A. Colombo), simone.sarasso@unimi.it (S. Sarasso).

https://doi.org/10.1016/j.neuroimage.2019.01.024
Received 24 September 2018; Received in revised form 20 December 2018; Accepted 9 January 2019
Available online 11 January 2019

1. Introduction

In clinical practice, behavioural unresponsiveness is often interpreted as indirect evidence for the absence of consciousness (Giacino et al., 2004; Jones, 1979). Accordingly, behavioural unresponsiveness induced by general anesthesia is commonly associated with loss of consciousness. However, multiple lines of evidence support the notion that consciousness can be preserved in subjects who are disconnected from the environment—due to a blockade of sensorimotor pathways—thus pointing to behavioural unresponsiveness as an unreliable marker of the absence of consciousness (Sanders et al., 2012). Therefore, the development of an objective neurophysiological marker of consciousness, independently from behavioural responsiveness, is deemed necessary (Koch et al., 2016).

1.1. Unconsciousness is linked to EEG slowing, yet oscillations are unspecific for unconsciousness

A typical electrophysiological feature associated with the fading of consciousness is a redistribution of EEG spectral power from higher to lower frequencies, a phenomenon known as 'EEG slowing' (Oken et al., 2006; Steyn-Ross et al., 2004). This phenomenon has been observed during the transition from wakefulness to sleep (Merica and Blois, 1997; De Gennaro et al., 2001; Ogilvie, 2001), during anesthetic-induced loss of consciousness (as reviewed in (Brown et al., 2010)) and in severe disorders of consciousness (Chennu et al., 2014; Estraneo et al., 2016; Sitt et al., 2014; Coleman et al., 2005; Lechinger et al., 2013).

However, beyond an overall frequency slowing, different anaesthetics are associated with the emergence of different oscillatory peaks in the power spectral density (PSD). More generally, peaks of the PSD, reflecting oscillations in different frequency bands, can occur across vigilance states: theta rhythm during drowsiness (Finelli et al., 2000; Hung et al., 2013), REM sleep, ketamine anesthesia, sevoflurane anesthesia; alpha rhythm in eyes closed wakefulness, drowsiness, REM sleep, propofol or sevoflurane anesthesia; sigma rhythm during quiet wakefulness, deep NREM sleep, benzodiazepines sedation; high-beta rhythms during ketamine-anesthesia and REM sleep (Purdon et al., 2015; Cantero et al., 2002). The presence of such oscillations might have hindered the attempts to develop a general and reliable neurophysiological marker of unconsciousness based on EEG spectral power (Purdon et al., 2015). On the other hand, promising EEG measures based on effective connectivity (Juel et al., 2018) and multi-scale temporal complexity (Miskovic et al., 2018) have been recently proposed. Interestingly, the latter was associated with the spectral exponent, a measure that captures the overall slowing of the EEG across frequencies, while being minimally influenced by oscillatory peaks.

1.2. Non-oscillatory, 1/f-like activity constitutes the background of neurophysiological signals

Underneath oscillatory peaks, the 'background' of the PSD decays from slower to faster frequencies, according to an inverse power-law, with a 1/f-like shape (He et al., 2010). The spectral exponent—estimated from the slope of the PSD in log-log coordinates—indexes the steepness of the decay of the PSD background. This background could originate from truly arrhythmic activity (Juel et al., 2018), or from quasi-periodic activity (brief oscillations that vary in frequency), measured over a broad spatial or temporal scale (Palva and Palva, 2018). Whatever the precise origin of the 1/f-like shape, similar inverse power-law behaviour has been observed for neural activity across different spatial-scales (He, 2014), e.g. in membrane potential fluctuations (Destexhe et al., 2003), in local field potentials (Milstein et al., 2009; Buzsáki and Mizuseki, 2014), in electrocorticography (ECoG) (He et al., 2010; Miller et al., 2009; Manning et al., 2009; Freeman and Zhai, 2009), in magnetoencephalography (MEG) (Novikov et al., 1997; Dehghani et al., 2010), and fMRI (He, 2011; Ciuciu et al., 2012).

1.3. The EEG spectral exponent is linked to the balance between excitation and inhibition

The spectral exponent has been recently linked to the balance between excitation and inhibition in neuronal signalling, using one in-silico and three different in-vivo models (Gao et al., 2017). In one of these models, the spectral exponent reliably tracked the induction and the recovery from propofol-anesthesia in a pharmacological experiment with macaques (Gao et al., 2017).

Physiologically, the balance between excitation and inhibition changes dramatically during sleep. Consistently, the spectral exponent of the EEG diminishes with sleep depth, displaying more negative values as sleep deepens (Miskovic et al., 2018; Pereda et al., 1998; Robinson et al., 2001; Shen et al., 2003). The spectral exponent observed in slow-wave sleep was substantially more negative than in wakefulness, both in EEG (Freeman, 2006) and ECoG recordings (He et al., 2010; Freeman and Zhai, 2009). Interestingly, the spectral exponent of the only ECoG recording obtained during REM sleep had a similar value to those of wakefulness (He et al., 2010). This observation is consistent with the observation in rats of a steeper PSD decay during NREM sleep, as compared to that of REM and wakefulness (Leemburg et al., 2018). Another study found slightly more negative EEG spectral exponent values during sleep onset with respect to quiet wakefulness, as well as a decrease of the exponent over time, as sleep onset progressed (Šušmáková, 2006). Furthermore, the PSD of the EEG became progressively steeper from REM sleep, through sleep stage 2, to slow-wave sleep (Miskovic et al., 2018; Pereda et al., 1998; Shen et al., 2003).

In sum, vigilance states commonly associated with the presence of consciousness (wakefulness, REM, sleep-onset period)—despite variable degrees of sensorimotor connectedness—were characterized by a similar shallow decay of the PSD. In contrast, deep sleep and anesthesia-induced loss of consciousness steepened the decay of the PSD.

Thus, we hypothesized that, irrespectively of the presence of oscillatory spectral peaks, a common change happening during anesthetic-induced loss of consciousness is that the broad-band background shape of the PSD becomes more narrow and steep, yielding more negative values of the spectral exponent β. For this purpose, we employed three anesthetic agents with different and complementary mechanisms of action—namely xenon, propofol and ketamine—at high doses, individually tailored to render participants equally unresponsive. We then investigated drug-specific effects on the EEG spectral exponent β. Moreover, we evaluated the effectiveness of β in discriminating the presence/absence of conscious experience—based upon reports assessed either immediately or upon awakening from unresponsiveness. Finally, we assessed how the resting-EEG spectral exponent correlated with the Perturbational Complexity Index (PCI), acquired contextually in the same subjects (Sarasso et al., 2015). PCI is based upon the evoked EEG response to transcranial magnetic stimulation (TMS), and represents another marker of consciousness, independent of sensory processing and behavioural responsiveness (Casali et al., 2013; Casarotto et al., 2016).

2. Materials and methods

2.1. Participants

Data analysed in the present paper are taken from a previous study (Sarasso et al., 2015). In the current study, fifteen healthy participants (5 males, age 18–28 years) were randomly assigned to one of the three experiments (N = 5 for propofol, xenon, and ketamine, respectively). All participants gave written informed consent. The experimental protocol was approved by the local ethical committee of the University of Liège (Belgium). Before the experiment, medical history and physical examinations were performed to exclude medical conditions that were incompatible with anesthesia.

2.2. Experimental design

All experimental procedures were performed at the Centre Hospitalier Universitaire (CHU) in Liege, Belgium. Following drug administration, repeated assessments of responsiveness were performed at 30-s intervals using the Ramsay scale (Ramsay et al., 1974). Spontaneous EEG, followed by TMS-EEG recording, was performed before drug administration during the responsive wakefulness condition (Ramsay Scale score 2) as well as upon reaching deep unresponsiveness in three consecutive assessments (Ramsay Scale score 6, corresponding to no response to external stimuli) (Ramsay et al., 1974). During wakefulness, eyes were kept open (Weo) or closed (Wec) consistently with the anesthesia condition: closed during xenon and propofol anesthesia, open during ketamine anesthesia. TMS-EEG procedures, pre-processing and analysis (reported in (Sarasso et al., 2015)) yielded a single value for each recording (PCI, see below).

At the end of the TMS-EEG recordings, anesthesia was discontinued, participants were allowed to recover, and assessments of responsiveness were continued every 30 s. In the event of nausea caused by the anesthetic drug, participants were given metoclopramide (2 mg) to minimize possible complications. In addition, participant's electrocardiogram, non-invasive blood pressure, SaO2, exhaled CO2, and axillary skin temperature were continuously monitored.

2.3. 'Conscious report' and 'no report'

In order to assess the presence/absence of conscious experience during anesthesia-induced behavioural unresponsiveness, retrospective reports were collected in all participants after awakening. For this purpose, after participants recovered responsiveness (as assessed by three consecutive Ramsey Scale score 2 evaluations), they were asked to report their previous conscious experience ("what was going on through your mind before awakening?"). Experience was defined as "any kind of mental activity," which included thoughts, dreams, images, emotions, etc. Responses were recorded and lumped into two categories: 1) '**No report**': this category included cases where no conscious experience was reported, or no explicit recall was possible. One participant reported the feeling of having felt something just prior awakening from Xenon anesthesia—thus several tens of minutes after the end of the resting-EEG recording—but no explicit recall was possible; 2) '**Conscious report**', when the participant could describe the content of the experiences. Long, vivid and emotionally intense experiences, with an explicit narrative structure, were reported from all participants awakening from ketamine anesthesia. An example report of ketamine-dreams can be found in (Sarasso et al., 2015). While we cannot rule out that retrograde amnesia or confabulation upon awakening affected reports, the collection of retrospective reports remains the only available option to assess consciousness beyond responsiveness. Dream reports are indeed commonly employed to study mentation during sleep (Hobson et al., 2000; Siclari et al., 2017).

2.4. Anesthetic procedures

Given that the depth of anesthesia is hard to compare when using compounds acting on different molecular targets, the anesthetic procedures for the three experiments were aimed at reaching a common behavioural state, i.e. unresponsiveness, systematically assessed by means of repeated Ramsey Scale administrations. Thus, we attained Ramsay Scale score 6 for all the subjects in the three experiments by employing anesthetic procedures based on previous works. Specifically, for propofol anesthesia see (Murphy et al., 2011), for xenon see (Rex et al., 2006), while for ketamine we adopted induction procedures similar to (Lee et al., 2013) and anesthesia maintenance following several reports, as reviewed in (Miller et al., 2011).

Propofol. Propofol anesthesia was induced by a certified senior anesthesiologist through an intravenous catheter placed into a vein of the right hand or forearm. Throughout the study, the subjects breathed spontaneously, and additional oxygen (5 L/min) was given through a loosely fitting plastic face mask. Anesthesia was obtained with a target-controlled infusion (Alaris TIVA; CareFusion). The pump was controlled by a software algorithm based on the Marsh adult pharmacokinetic model for propofol (Marsh et al., 1991) set at 3 μg/ml. When the appropriate effect site concentration was reached, a 5-min equilibration period was allowed to ensure equilibration of propofol repartition between compartments.

Xenon. Xenon anesthesia was induced by a certified senior anesthesiologist. Before xenon administration, we performed a denitrogenation with 100% oxygen applied via a facial mask. Once completed, a 2–3 mg/kg bolus of propofol was administered through a right arm or forearm intravenous catheter in order to allow the insertion of a laryngeal mask securing the airway. Xenon was then introduced progressively and propofol was withdrawn. We then waited for spontaneous reduction of plasmatic propofol concentration (propofol washout) until calculated propofol plasma concentration were below 1 μg/ml (Rex et al., 2006), within a subanesthetic range (Fiset et al., 1999) after which anesthesia was maintained with xenon ($62.5 \pm 2.5\%$ in oxygen) using a Dräger PhysioFlex closed circuit ventilator (Dräger; Luebeck, Germany). Participants were undergoing assisted spontaneous ventilation with pressure control maintaining normocapnia and received a total amount of xenon ranging from 24 to 32 L.

Ketamine. Ketamine anesthesia was induced by a certified senior anesthesiologist using a 2 mg/kg intravenous infusion (diluted in 10 mL of 0.9% normal saline) of racemic ketamine (Ketalar®, Pfizer Ltd, Istanbul, Turkey) over 2 min and maintained by continuous ketamine infusion at 0.05 mg/kg/min (Baxter infusion pump AS40A; Baxter Healthcare Corp., Deerfield, IL) over the entire experimental procedures.

2.5. EEG acquisition and preprocessing

EEG measurements were performed using a 60-channel EEG amplifier (Nexstim Plc., Finland). EEG signals were referenced to an additional electrode on the forehead, online filtered (0.1–350 Hz) and sampled at 1450 Hz. Two extra sensors were used to record the electrooculogram. Impedance at all electrodes was kept below 5 kΩ. Raw EEG signals are made available online upon request, at the repository Zenodo (https://doi.org/10.5281/zenodo.806176). EEG signals were offline filtered in forward and reverse direction with a high-pass (cutoff: 0.5 Hz) and a low-pass (cutoff: 60 Hz) 5th order Butterworth IIR filter. Supplementary analysis was performed without any additional temporal filters (see Supplementary Material, section 1), in order to consider frequencies below 1 Hz. Bad channels were rejected based on visual inspection ($\leq$10% of channels per recording). Rejected channels were then interpolated using spherical splines. Continuous data was segmented (2 s length) and artifactual epochs were rejected following visual inspection. In addition, to minimize the influence of electromyographic (EMG) and electrooculographic (EOG) activity, ICA decomposition was performed; components were visually inspected with respect to their topography, their time-series and their PSD. ICA components resembling EMG activity (large high-frequency power relative to low frequency power, highly localized scalp-origin—i.e. high spatial kurtosis—and EMG-like temporal structure—i.e. spiking activity), as well as those resembling EOG activity (temporally sparse and sharp activation, pre-frontal topography and either symmetric or asymmetric polarity, corresponding to blinks or eye movements) were identified. Artifactual components were removed (xenon: mean $\pm$ std, $7.20 \pm 3{,}19$; propofol: 8.40 ± 3.36; ketamine: 22.6 ± 8.62; Wakefulness with eyes open: 21.60 ± 7.76; Wakefulness with eyes closed: 19.70 ± 5.06), and the residual components were back-projected to the electrode space. Only the first 5 min of available clean data were considered for further analysis.

Besides the manual cleaning procedure described above, we performed in parallel an automated-cleaning procedure, in order to assess the feasibility of a fully-automated processing pipe-line yielding the

spectral exponent. We then performed the same analysis described in the main text, and replicated the results (See Supplementary Material, section 2).

2.6. Estimation of the spectral exponent from the PSD background

The power spectral density (PSD) was estimated at each electrode (see topographies in Supplementary Fig. 5) using the Welch's method, with a Hanning windows of 2 s and 50% overlap. The linear trend within each window was removed prior to spectral estimation, to avoid the bias due to low frequencies outside the frequency range under scrutiny.

The PSD background (i.e. non-oscillatory) decays approximately according to an inverse power-law: $PSD(f) \sim 1/f^{\alpha}$ (Pritchard, 1992); here we report the spectral exponent $\beta = -\alpha$. The spectral exponent is thus equivalent to the slope of a linear regression of the PSD, fit after taking the logarithm of both the x and y axis. However, when linearly-spaced frequency bins are considered under a logarithmic scale, bins in higher-frequencies become progressively more dense, and thus gain disproportionate weight with respect to lower frequency-bins in a subsequent linear regression (Hwa and Ferree, 2002). To avoid this potential bias, we up-sampled the PSD curve with logarithmically spaced frequency bins (such that the upsampled PSD had 4 times the number of datapoints than the original PSD), resulting in equally-spaced frequency bins under logarithmic scale, required to properly estimate the spectral exponent.

To intuitively illustrate how changes in the spectral exponent relate to changes in the temporal properties ('smoothing' and 'slowing') of the EEG, an EEG signal recorded during wakefulness is filtered so as to obtain progressively more negative spectral exponents (Fig. 1). Filtering consisted in taking the Fourier transform of the signal, changing the slope of the PSD (PSD rotation), then reconstructing the signal via the inverse Fourier transform. Here, PSD rotation was obtained by multiplying the PSD by $1/f^{\beta}$, with β spanning from 0 to 1 (green to black signal in Fig. 1), then dividing the PSD by its mean.

The exact peak frequency of the oscillations can vary across individuals, and the bandwidth can change across the scalp (Klimesch et al., 2007). For this reason, rather than defining a priori the frequency bands that deviate from a power-law behaviour, we defined these bands following a data-driven procedure. A **three-step procedure** was conceived in order to estimate the spectral exponent β of the background PSD, while discarding frequencies exhibiting oscillatory peaks. **1)** A first least-square line was fit to the PSD, under double-logarithmic axis. **2)** Frequency bins with large positive residuals (larger than 1 median absolute deviations of the residual distribution) were considered as likely containing oscillatory peaks. The contiguous frequency bins with positive residuals were considered as part of the base of the peak, and thus removed from subsequent analysis. **3)** A second least-square line was then fit on the remaining frequency bins (i.e. those consistent with a power-law behaviour). The slope of this second line corresponded to the spectral exponent β of the PSD background (Fig. 2). The spectral exponent at each electrode was relatively homogenous across the scalp within conditions (Supplementary Fig. 5). In order to obtain a single estimate of the spectral exponent across the scalp, the average spectral exponent across electrodes was considered for each participant for all subsequent analysis. The Matlab code to estimate the spectral exponent is available online: https://github.com/milecombo/spectralExponent/blob/master/README.md.

We corroborated the proposed three-step procedure by performing supplementary analysis with a previously published method—Irregularly Resampled AutoSpectral Analysis (IRASA)—aimed at isolating the fractal (non-oscillatory) component of the PSD (Wen and Liu, 2016). The two procedures yielded highly similar spectral exponents (Supplementary Material, section 1; Supplementary Fig. 2).

2.7. Broad-band spectral exponent

Using this method, we first estimated the overall spectral exponent for a broad frequency range (1–40 Hz) (Fig. 2A). We avoided to fit the slope for frequencies below 1 Hz, due to the sensitivity of the EEG at these frequencies to slow-drifts of the signal, movement artifacts and high-pass filter-attenuations. Accordingly, we set a high-pass filter cutoff at 0.5 Hz. We also avoided to fit the slope for frequencies above 40 Hz due to the sensitivity of the EEG at these frequencies to potential muscle artifacts—although these were already minimized by the ICA cleaning (see Method, section 2.5).

2.8. Sub-bands: low-band and high-band spectral exponent

A subsequent closer examination of the PSD decay revealed a 'knee' at ~20 Hz (evident in Figs. 2 and 3A). In order to obtain a better local fit, we therefore split the broad 1–40 Hz band in two equally spanning sub-bands for additional analysis, obtaining a 'low-band' (1–20 Hz, Fig. 2B), and a 'high-band' (20–40 Hz, Fig. 2C). For all conditions of wakefulness (N = 15), the low frequency range displayed a flatter slope with respect to the high frequency range: mean ± std, −0.80 ± 0.29 and −2.55 ± 0.93 respectively, $T(14) = 5.78$, $P = 4*10^{-5}$. These two sub-

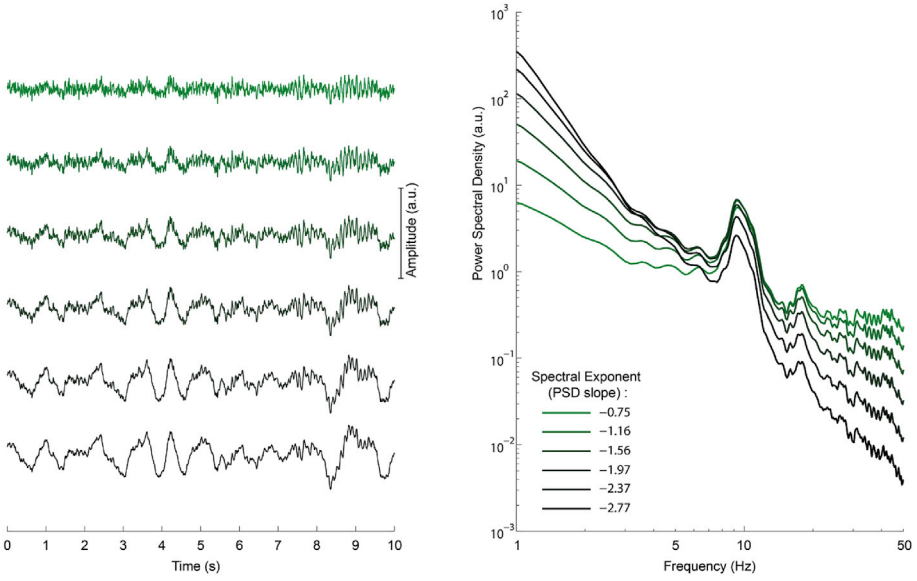

Fig. 1. A more negative broad-band spectral exponent (β) indexes a steeper power spectral density (PSD) decay, related to a 'slower' and 'smoother' temporal profile of the EEG signal. As β decreases, the amplitude of high frequencies becomes smaller relative to the amplitude of low frequencies ('EEG slowing'). To illustrate this concept, an EEG signal (recorded during wakefulness, green) is progressively filtered, so as to reduce its broad-band spectral exponent (darker colors). Filtering is obtained by taking the Fourier transform of the original signal, changing the slope of the PSD (PSD rotation), then reconstructing the signal via the inverse Fourier transform. The temporal profile of each signal is shown on the left panel (only 10 s out of 5 min are shown); the relative PSD, estimated with the Welch's method, is shown on the right panel. Note the appearance of slow waves and the reduction of high-frequency activity—typical signatures of the loss of consciousness during general anesthesia—as the PSD becomes progressively steeper.

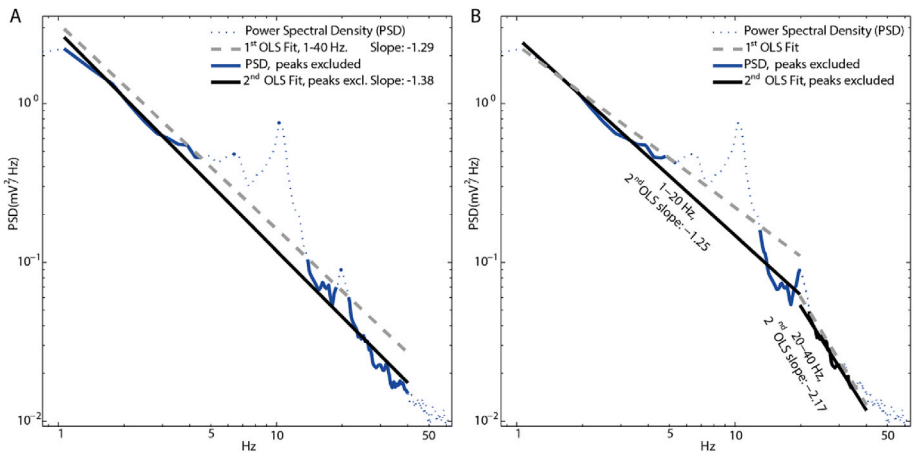

Fig. 2. The background of the Power Spectral Density of the EEG decays according to an inverse power-law: PSD(f) ~$1/f^{\alpha}$, with $\beta = -\alpha$. The spectral exponent β indexes the steepness of the decay of the PSD background. Oscillations (Theta, Alpha, Beta) appear as peaks above the Power Spectral Density (PSD) background, and thus deviate from the overall 1/f shape. A three-step fitting procedure is devised to discard oscillatory peaks, prior estimating the background slope. Fitting is done separately for three frequency ranges: broad-band (1–40 Hz, **A**), low-band (1–20 Hz, **B**, left) and high-band (20–40 Hz, **B**, right). 1) Fit a first OLS line to the PSD (gray dashed line), in log-log coordinates. 2) Identify and discard frequency bins around oscillatory peaks (bins with large positive residuals, >1 median absolute deviation). Adjacent bins with positive residuals are also discarded, so as to discard both the top and the base of the peak (thin blue dotted line). 3) Fit a second OLS line (thick black line) to the remaining frequency bins. The slope of this second line corresponds to the spectral exponent.

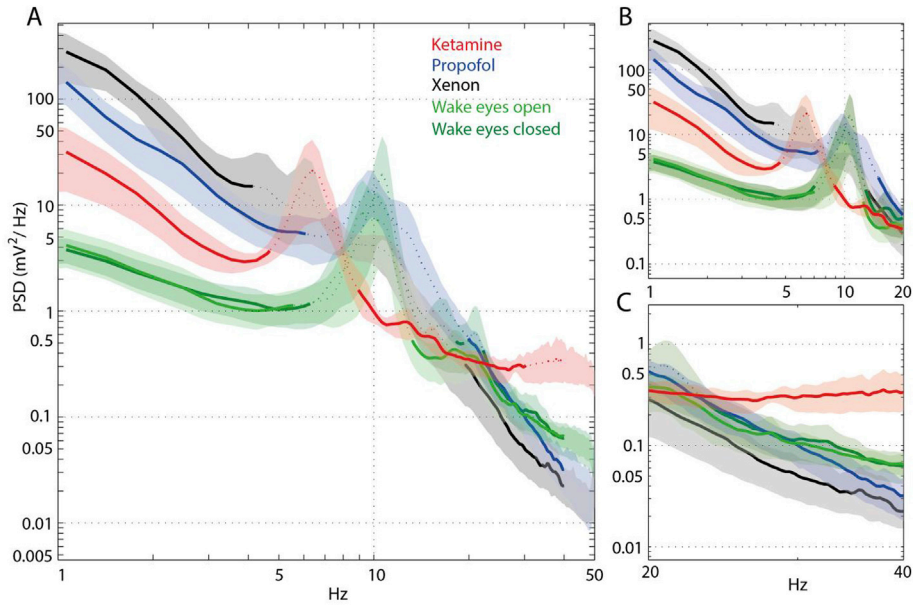

Fig. 3. The background of the PSD decays differently across conditions. EEG was recorded during wakefulness and anesthesia in three groups of healthy participants, undergoing a specific anesthetic procedure; either: xenon (black) propofol (blue) or ketamine (red). During wakefulness, participants had their eyes open (light-green) or closed (dark-green) consistently with the anesthesia condition (open prior Ketamine, closed prior Xenon or Propofol). Each line shows the grand-average PSD across participants; the shaded area indicates the bootstrapped 95% confidence interval for the mean across participants. Frequency bins around oscillatory peaks (dotted line) deviate from the background power-law decay (solid line) of the grand-average PSD. We assessed whether frequency bins adhered or deviated from the background power-law trend, separately for the broad-band (1–40 Hz, **A**), for the low-band (1–20 Hz, **B**), and for the high-band (20–40 Hz, **C**). Note that in the main analysis, deviations from power-law behaviour were assessed for each participant at the single electrode level.

bands ultimately revealed a different response to pharmacological manipulations, as detailed in the Results, section 3 and in Fig. 3. The PSD and the frequency bins adhering to an inverse power-law behaviour are displayed for the grand-average across participants, in each experimental condition (Fig. 3A, B, C, respectively for the broad-band, the low-band and the high-band). As explained before, in the main analysis, the deviation from power-law behaviour at each frequency bin was assessed for each participant at the single electrode level. Nonetheless, deviations appeared at similar frequencies across electrodes and participants (Supplementary Material, section 3-5; Supplementary Figs. 6 and 7; Supplementary Table 1).

2.9. Repeated-measures ANOVA: specific effects of the anesthetics

In order to estimate the effect of each anesthetic on the spectral exponent, we conducted a repeated-measures ANOVA, for each frequency band (broad-band, low-band, high-band). The models had anesthetic (xenon, propofol, ketamine) as between-subject factor, and condition (wakefulness, anesthesia) as within-subject factor. To observe whether each anesthetic induced a consistent change across all the members of the group, we visualized the spectral exponents during wakefulness and anesthesia for each participant (Fig. 4A). For each frequency-band and anesthetic, we performed planned paired t-tests to contrast conditions (Table 1); p-values were accordingly corrected with the FDR procedure across bands and anesthetics.

2.10. Discriminant analysis: 'conscious report' vs 'no report'

Besides this, we were interested in determining how well the spectral exponent could discriminate states with conscious report from states where report was absent. The outcomes of the ANOVA analysis were not used to perform feature-selection, thereby we could perform a classification analysis on the same dataset—using a cross-validation scheme—without incurring in overfitting problems. The classes to be discriminated ('Conscious report', 'No report') were formed based upon subjective reports performed immediately during wakefulness or delayed upon awakenings from anesthesia (see section 2.3, as well as (Sarasso et al., 2015)). We therefore pooled all the EEG recordings of the xenon and propofol condition in the 'No report' class (N = 10), and all the EEG recordings during the wakefulness condition (irrespectively with eyes open, Weo, or eyes closed, Wec) and ketamine condition in the 'Conscious report' class (N = 20). We performed a linear discriminant

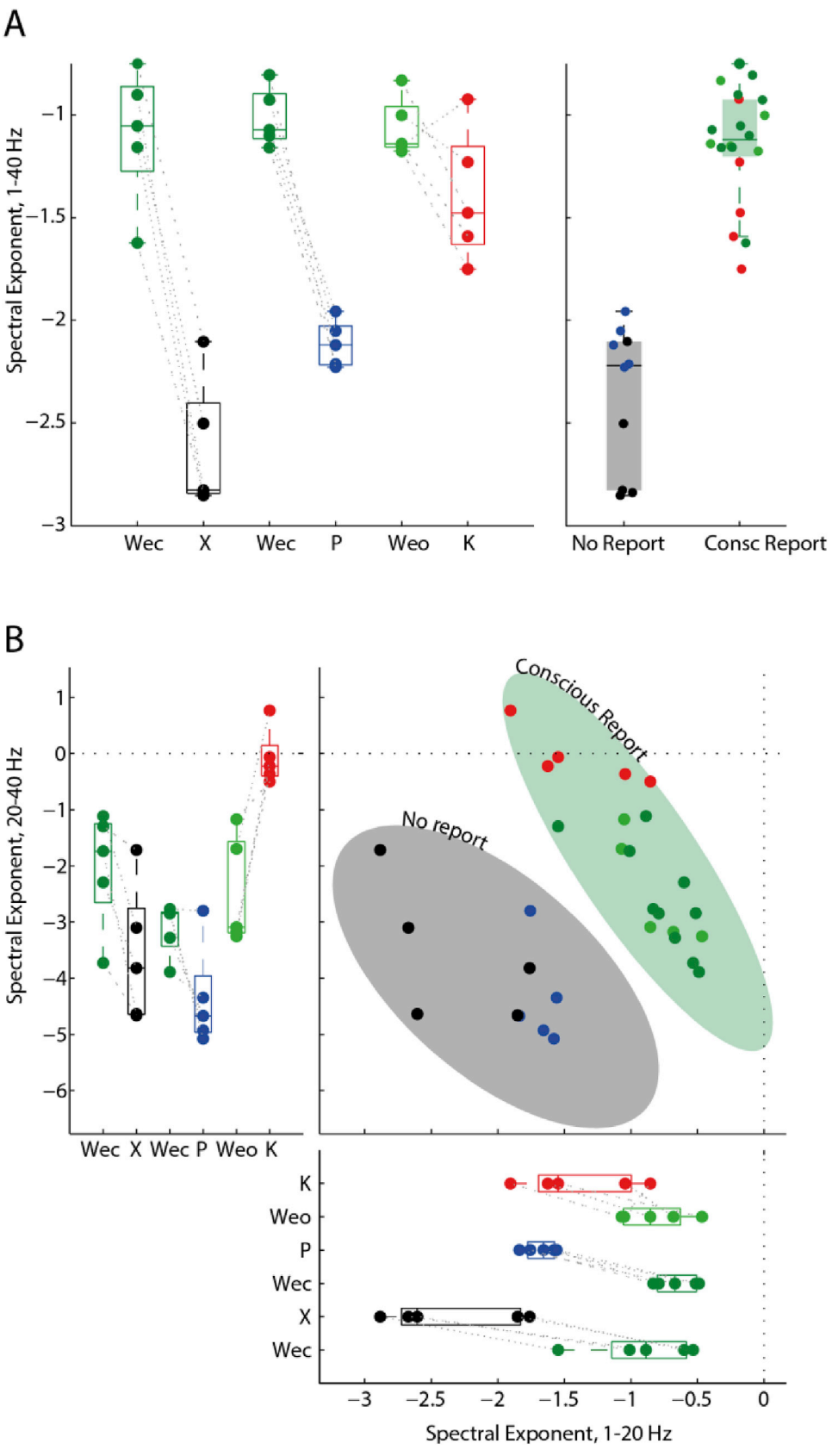

Fig. 4. The spectral exponent reliably separates conditions where a conscious report could be obtained (wakefulness, ketamine) from conditions where no report could be obtained (xenon, propofol). Reports were assessed immediately (wakefulness) or upon recovery from unresponsiveness (anesthesia). **A)** The broad-band spectral exponent in the 'No report' class (xenon, propofol) decreases dramatically with respect to the 'Conscious report' class (wakefulness, ketamine), indexing a steeper decay of the background of the PSD. Boxplots and individual values of the spectral exponent are shown for each condition: wakefulness with eyes closed (Wec, dark-green), wakefulness with eyes open (Weo, light-green), xenon (X, black), propofol (P, blue), ketamine (R, red). Datapoints belonging to the same participant are connected by a dotted line. **B)** Considering the spectral exponent jointly over the low-band (1–20 Hz) and the high-band (20–40 Hz), reveals distinct regions for the 'No report' and the 'Conscious report' classes, as well as for each anesthetic-drug. Marginal plots, bottom and left, display for each participant the values of the spectral exponent in the low-band (1–20 Hz) and in the high-band (20–40 Hz) respectively. These values are displayed together as a joint distribution in the central plot, revealing that the two bands are negatively correlated within the 'Conscious report' and the 'No report' class. Ellipses represent the central 95% of a normal bivariate distribution, fitted to the data. The ellipse of the 'No report' class (X, P, black shaded area) does not overlap with that of the 'Conscious report' class (Wec, Weo, K, green shaded area).

Table 1

Spectral scaling exponents (β), estimated as the slope of the background of the PSD under log-log coordinates, after discarding peaks. The mean spectral exponent across electrodes was considered for each participant; condition-averages are reported below. P-values for the contrasts are reported both as raw uncorrected values (P-raw, in gray), and after the correction with the False Discovery Rate (FDR) procedure across anesthetics and frequency bands (P-FDR). Bold and italics respectively highlight significant ($P < 0.05$) and trend-level ($P < 0.1$) FDR-corrected P-values.

Spectral exponent β				
Condition	Anesthesia (mean std)	Wakefulness (mean std)	Contrast Anesthesia vs Wakefulness	
			T (df = 4)	(P-raw) P-FDR
Broad-Band (1–40 Hz)				
Xenon	−2.63 0.33	−1.10 0.33	−12.11	(0.0003) **0.0006**
Propofol	−2.11 0.11	−1.01 0.14	−12.31	(0.0003) **0.0006**
Ketamine	−1.40 0.32	−1.06 0.14	−2.13	(0.1006) 0.1006
Low-Band (1–20 Hz)				
Xenon	−2.36 0.51	−0.92 0.41	−13.01	(0.0002) **0.0006**
Propofol	−1.68 0.12	−0.66 0.16	−14.15	(0.0001) **0.0006**
Ketamine	−1.40 0.43	−0.82 0.26	−2.55	(0.0632) *0.0711*
High-Band (20–40 Hz)				
Xenon	−3.59 1.23	−2.03 1.05	−3.62	(0.0224) **0.0336**
Propofol	−4.36 0.92	−3.13 0.47	−2.84	(0.0467) *0.0600*
Ketamine	−0.08 0.50	−2.48 0. 97	5.38	(0.0058) **0.0104**

analysis (LDA) with a leave-one-out cross-validation scheme, to evaluate the accuracy, sensitivity, specificity, and area under the ROC curve (AUC-ROC) of the spectral exponent features in discriminating the 'Conscious report' class from the 'No report' class. We evaluated the performance of a single-feature classifier (broad-band spectral exponent) and a two-features classifier (the low-band and the high-band spectral exponents). We evaluated the degree of separation between classes obtained with the single-feature classifier vs the two-features classifier, by comparing the mean silhouette values (based upon Euclidean distances), and the t-values relative to the contrast of the two classes. These two statistics allowed to estimate which classifier was better, even when both classifiers had 100% accuracy. Furthermore, we characterized the spread of the datapoints within each class along the two largest directions of variation within the two-dimensional space of the two features (Fig. 4B). For this purpose, we plotted an ellipse centered in the centroid of the two features, oriented along the two principal directions of variation (eigenvectors), and whose width was set as the 5th and 95th percentile of a normal bivariate distribution with the mean and variance estimated from the observed data points. This procedure allowed us to visually appreciate if there was any significant overlap between the regions belonging to each class. We also computed the correlation coefficient within each class between the high and low frequency spectral exponent, in order to characterize their mutual relationship. To quantify the overlap between the two classes, we reported how many individual recordings occupied values more extreme (in the direction of the difference of the means of each condition) than the range of values occupied by the other condition of interest.

2.11. Supplementary discriminant analysis: ketamine vs wakefulness and xenon vs propofol

As a secondary aim, we furthermore evaluated the performance of the classifiers, with a single or with two-features, to discriminate specific conditions characterized by either the presence of reports—i.e. ketamine vs wakefulness—or the absence of retrospective reports—i.e. xenon vs propofol (see results in Supplementary Material, section 6).

2.12. Correlations of the spectral exponent with the perturbational complexity index

We furthermore assessed the relationship between two different neurophysiological markers of the level of consciousness, both independent from behavioural responsiveness. In order to do this, we computed the correlation across all individual recordings between the spectral exponent—based upon spontaneous EEG—and the Perturbation Complexity Index (PCI) —based upon the EEG response to TMS derived by a previous study (Sarasso et al., 2015). In brief, PCI gauges the amount of information contained in the integrated response to a direct perturbation—i.e. the spatiotemporal patterns of TMS-evoked cortical source activity. Specifically, PCI is calculated as the Lempel-Ziv complexity (cL) of the binarized activity sequence of length L, normalized by the corresponding source entropy H(L). PCI is thus computed as: $PCI = cL*\log_2 L / LH(L)$ (Casali et al., 2013).

3. Results

3.1. Repeated-measures ANOVA: specific effects of the anesthetics

The effect of the three anesthetics (xenon, propofol, ketamine) on the spectral exponent β was assessed by means of a repeated-measures ANOVA test, separately for the three frequency bands (broad-band, low-band and high-band). Planned t-contrasts of condition (wakefulness vs anesthesia) for each anesthetic were performed applying the False Discovery Rate (FDR) procedure to the resulting P-values, across anesthetics and across the three frequency bands (Table 1). For the broad-band spectral exponent, we observed a main effect of condition ($F(1,12) = 180.64$, $P = 1*10^{-8}$) and anesthesia-type ($F(2,12) = 11.76$, $P = 0.0015$), and a significant interaction effect ($F(2,12) = 22.60$, $P = 9*10^{-5}$). As compared to the wakefulness condition of each participant, the broad-band spectral exponent was reduced (indexing a steeper PSD decay) to a large extent during xenon and to a lesser extent during propofol, while it did not significantly change during ketamine (Figs. 3A and 4A, Table 1).

Results obtained for the low-band spectral exponent resembled those of the broad-band. Also in this case, we observed a main effect of condition ($F(1,12) = 136.14$, $P = 7*10^{-8}$) and anesthetic ($F(2,12) = 4.52$, $P = 0.0343$), and a significant interaction effect ($F(2,12) = 8.42$, $P = 0.0052$). Again, as compared to the wakefulness condition of each participant, the low-band spectral exponent was reduced to a large extent during xenon, to a lesser extent during propofol, while it did not significantly change during ketamine (Figs. 3B and 4B, Table 1).

On the other hand, for the high-band spectral exponent, we did not observe a main effect of condition ($F(1,12) = 0.26$, $P = 0.6177$), while we did observe an effect of anesthetic ($F(2,12) = 13.54$, $P = 8*10^{-4}$), as well as a significant interaction effect ($F(2,12) = 25.29$, $P = 5*10^{-5}$). Specifically, as compared to the wakefulness condition of each participant, the high-band spectral exponent decreased in xenon and in propofol, while it increased in ketamine (Figs. 3C and 4B, Table 1).

In sum, xenon and propofol largely decreased the spectral exponent across the two sub-bands in all participants; such decrease was therefore

also observed in the broad-band. In contrast, ketamine differently altered the spectral exponent in the two sub-bands—decreasing it in the low-frequency band (albeit only at trend-level) and increasing it in the high-frequency band. Notably, these two opposite changes yielded a broad-band spectral exponent that was overall similar to that observed during wakefulness (Figs. 3A and 4A).

3.2. Discriminant analysis: 'conscious report' vs 'no report'

For the main aim, we discriminated conscious states from states where consciousness was greatly reduced or absent, based on the EEG spectral exponent features. We hereby consider the average performance across partitions in discriminating the 'Conscious report' class (wakefulness, ketamine) from the 'No report' class (xenon, propofol), for the single-feature (broad-band spectral exponent) and the two-features classifier (low- and high-band spectral exponents). The single-feature classifier, yielded 100% accuracy, sensitivity and specificity, and the area under the receiver operating characteristic curve (AUC-ROC) was equal to 1. Similarly, the classifier with two-features, yielded 100% accuracy, sensitivity and specificity, and the AUC-ROC was equal to 1. A larger distance between 'Conscious report' and 'No Report' class could be observed when considering two features jointly (Fig. 4B) as compared to when using a single feature (Fig. 4A), as indexed by a larger silhouette value (0.7930 vs 0.6836), and by a larger t-value (13.22 vs 10.16 respectively).

We then considered the overlap between the spectral exponent values of these two classes, reporting how many individual recordings occupied values that were more extreme (in the direction of the difference of the means of each condition) than the range of values occupied by the other condition of interest. The spectral exponent in the 1–40 Hz of the 'No report' class ($N = 10$), as compared to the 'Conscious report' class ($N = 15$), was largely more negative (β, mean ± std, 'No report': -2.37 ± 0.35; 'Conscious report': -1.14 ± 0.28) in all 10 recordings (Fig. 4A). Furthermore, the spectral exponent of the 'No report' class was more negative ('No report': -2.02 ± 0.50; 'Conscious report': -0.95 ± 0.41) in 3 recordings for the 1–20 Hz, while it was more negative ('No report': -3.97 ± 1.10; 'Conscious report': -1.93 ± 1.38) in 6 recordings for the 20–40 Hz (Fig. 4B).

There was a negative correlation between the low and high spectral exponents in the 'Conscious report' condition ($R = -0.85$, $P = 2*10^{-6}$) and, although only at trend-level, in the 'No report' class ($R = -0.61$, $P = 0.0608$). Consistently, the main direction of variance was similar for both the 'Conscious report' and the 'No report' class, as depicted by the ellipses in Fig. 4. The data-points of the two classes occupied separate regions in the two-dimensional space formed by the two features. Furthermore, there was no overlap between the ellipses of the two classes, each covering the central 95% of a normal distribution with mean and standard deviation estimated from the datapoints of each class.

3.3. Supplementary discriminant analysis: ketamine vs wakefulness and xenon vs propofol

After discriminating the 'Conscious report' from the 'No report' class, we tested the ability of the spectral exponent β to discriminate specific conditions within each class characterized by either the presence of reports—i.e. ketamine vs wakefulness—or the absence of retrospective reports—i.e. xenon vs propofol. Results are detailed in the Supplementary Material, section 6). In sum, the broad-band spectral exponent did not distinguish ketamine anesthesia from resting wakefulness (Fig. 4A). When the low- and high-band spectral exponents were jointly considered (Fig. 4B), ketamine could be distinguished from resting wakefulness, due to a spectral exponent that was largely overlapping in the 1–20 Hz range and smaller in the 20–40 Hz range. Furthermore, xenon could be partially distinguished from propofol by a steeper spectral exponent both in the 1–20 Hz as well as in the 1–40 Hz range (Fig. 4).

3.4. Correlation of the spectral exponent with the perturbational complexity index

Finally, we assessed the overall correlation between the spectral exponent and an established measure of the level of consciousness—perturbational complexity index, PCI— derived from the EEG responses to TMS (Fig. 5). PCI was highly correlated with the spectral exponent across all recording sessions, most prominently for the broad-band ($R = 0.86$, P-raw $= 1*10^{-9}$, P-corrected $= 3*10^{-9}$), as well as for the low-band ($R = 0.76$, P-raw $= 1*10^{-6}$, P-corrected $= 2*10^{-6}$) and less so (although significantly) for the high-band ($R = 0.51$, P-raw $= 0.0041$, P-corrected $= 0.0041$). Thus, even though the correlation of PCI with the 20–40 Hz spectral exponent was smaller than that with the 1–20 Hz spectral exponent, PCI correlated the most with the spectral exponent of a

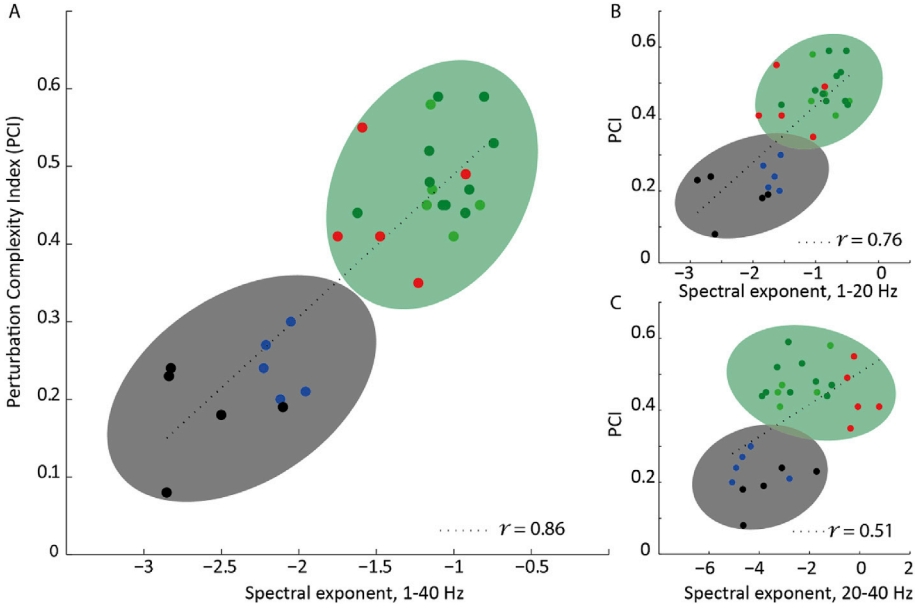

Fig. 5. The spectral exponent at rest is robustly correlated to the complexity of the TMS-evoked response, as assessed by Perturbation Complexity Index (PCI). PCI is an empirical measure that is maximized by the joint presence of integration and differentiation, a fundamental requirement for the emergence of consciousness. Both PCI and the spectral exponent peaked for the 'Conscious report' class (wakefulness, dark and light green dots; ketamine anesthesia, red dots) and were the lowest for the 'No report' class (propofol anesthesia, blue dots; xenon anesthesia, black dots). Although PCI correlated better with the low-band exponent (1–20 Hz, B) than with the high-band exponent (20–40 Hz, C), the best correlation is obtained with the broad-band exponent (1–40 Hz, A), suggesting that PCI is related to the scaling properties of a broad range of frequencies. A linear-fit across all datapoints is shown as a dotted line. Ellipses represent the central 95% of a normal bivariate distribution, fitted to the data. The orientation of the ellipses reveal the direction of largest variation of the data-points within each class.

broad 1–40 Hz band, encompassing both the low- and high-band.

4. Discussion

In the present work, we aimed to assess how anesthesia, induced by three anesthetics with distinct mechanisms of action, changed the overall decaying shape of the PSD of the resting EEG. Specifically, the steepness of the PSD decay was indexed by the spectral exponent β, once spectral peaks were removed. Furthermore, based on β, we aimed to objectively discriminate states in which conscious experience occurs—'Conscious report'—such as during wakefulness or ketamine anesthesia, from states in which consciousness is greatly reduced or absent—'No report'—such as during xenon or propofol anesthesia. Participants regaining responsiveness from either propofol or xenon anesthesia did not report any conscious experience during the unresponsive period. However, participants regaining responsiveness from ketamine anesthesia confirmed having had conscious experience, reporting long and vivid dream-like psychedelic experiences while disconnected from the external environment, in line with previous subjective reports (Bowdle et al., 1998; Brown et al., 2011; Gouzoulis-Mayfrank et al., 2005; Kiefer et al., 2008). During wakefulness, the PSD of the resting EEG decayed approximately as f^{β} ($\beta \sim -1$) over a broad frequency range, consistently with previous EEG observations (Dehghani et al., 2010; Pereda et al., 1998; Šušmáková, 2006). The broad-band spectral exponent remained approximately unchanged during ketamine anesthesia, consistent with the presence of conscious reports. On the other hand, the absence of conscious reports following both xenon and propofol anesthesia was associated with a sharp decrease of the broad-band spectral exponent in all participants, indexing a steeper PSD decay (Figs. 3A and 4A).

4.1. PSD decay and activity propagation

A steepening of the PSD was previously observed, among other results, in a computational model of general anesthesia, due to the blockade of network activity propagation (Zhou et al., 2015). A single parameter controlled the probability of percolation of stochastic activity through a hierarchical network. Below a certain probability threshold, the network-activity underwent a sharp transition, which resembled the rapid loss of consciousness occurring within a narrow anesthetic concentration. Indeed, the simulated EEG rapidly slowed, becoming more regular, and the PSD steepened. Accordingly, a steepening of the PSD, as measured by a more negative spectral exponent, was also associated with reduced entropy at short-time scales across the wake/sleep cycle (Miskovic et al., 2018). Reduced entropy at short-time-scale indexes more regular local brain dynamics, underpinned by increased synchronization of neuronal assemblies.

The scaling of the PSD could be explained by mechanisms based upon stochastic activity and different filtering properties of extracellular media (Bédard et al., 2006). Alternative proposals provide a functional explanation for 1/f behaviour and the steepening of the PSD. Specifically, the steepening of the PSD could result from the dampening of activity propagation mediated by refractory periods, as modelled in a simulated network with only excitatory neurons (Freeman and Zhai, 2009).

Recently, a more realistic model, including both excitatory and inhibitory populations, further pointed to the crucial role of blocking activity propagation in steepening the PSD decay (Gao et al., 2017). In this case, a network simulating LFP activity received stochastic inputs from both an excitatory and an inhibitory population, each with a particular conductance profile. The current fluctuations of the input from the inhibitory population, compared to those from the excitatory population, had a steeper PSD-decay. Thus, when increasing the contribution of the inhibitory population, relative to that of the excitatory one—i.e. by reducing the excitation/inhibition (E/I) ratio—the PSD of the simulated-LFP also steepened its decay. This prediction was verified in different experimental set-ups, within the same study (Gao et al., 2017). Indeed, the E/I balance modified the PSD-slope in LFP recordings in the rat hippocampus, when considering temporal excitability fluctuations driven by theta-cycle, as well as spatial changes in inhibitory synaptic density. Furthermore the PSD of macaque ECoG became steeper during propofol-induced loss of consciousness—as here reported—and its temporal changes well matched the time-course of anesthetic action. This study therefore provides a mechanistic explanation for changes in the spectral exponent across the induction of- and recovery from-anesthesia, in terms of global changes in the balance between excitation and inhibition.

Furthermore, as during physiological sleep the E/I balance shifts towards inhibition, EEG activity is characterized by a steeper PSD decay over a broad range of frequencies (Miskovic et al., 2018; He et al., 2010; Freeman and Zhai, 2009; Pereda et al., 1998; Freeman, 2006; Šušmáková, 2006). In sum, pharmacological, physiological as well as computational evidence show that changes in the E/I balance result in changes in the spectral exponent, estimated over a broad range of frequencies, encompassing those under scrutiny in the current study.

4.2. Activity propagation, E/I balance and the capacity for consciousness

Multiple empirical observations indicate that a marked alteration of neuronal activity propagation, mainly regulated by the E/I balance, could impede the emergence of consciousness. On the one hand, low E/I may lead to unconsciousness—as in barbiturate anesthesia (Scott et al., 2014), propofol anesthesia (Solovey et al., 2015; Tagliazucchi et al., 2016), or deep sleep (Kantelhardt et al., 2015; Meisel et al., 2017; Tagliazucchi et al., 2013; Priesemann et al., 2013). On the other hand, high E/I may also lead to unconsciousness, as during epileptic seizures (Meisel et al., 2012; DiNuzzo et al., 2014) and during xenon anesthesia (Hirota, 2006). In either case, states where consciousness is greatly impaired or abolished are characterized by rather excessive or insufficient propagation of activity (Tagliazucchi, 2017). Consistently, in our study, both xenon and propofol anesthesia markedly reduced or abolished conscious experience.

Conversely, the waking brain normally operates in a state where activity is at the edge of extinction, such that the propagation of activity is approximately balanced, yet slightly over-compensated by dampening mechanisms, i.e. slightly skewed towards inhibition. This idea is supported by theoretical work (Carhart-Harris et al., 2014; Pearlmutter and Houghton, 2009), and by multiple lines of experimental evidence (Priesemann et al., 2014; Hahn et al., 2017). Therefore, there is room for an increase in excitation—such as that induced by glutamate release mediated by classical psychedelic drugs, e.g. LSD, and dissociative anesthetics, e.g. Ketamine (Preller and Vollenweider, 2018)—while keeping the E/I still approximately balanced, and preserving the capacity for consciousness (Carhart-Harris et al., 2014). Consistently, in our study, ketamine, even at anesthetic doses, preserved the capacity for consciousness.

We now consider in depth the relationship between changes in the spectral exponent and the specific mechanism of action of each anesthetic.

4.3. Spectral exponent and mechanisms of action: propofol

In the current study, propofol induced a prominent slowing of the EEG across the 1–40 Hz range, as indexed by a more negative spectral exponent in the broad-band, as well as in both the low and high frequency bands (Figs. 3 and 4, Table 1). The induction of a prominent alpha oscillation (Fig. 3A, Supplementary Figs. 6 and 7) is well documented in previous work on propofol anesthesia (Purdon et al., 2015; Murphy et al., 2011; Scheinin et al., 2018a); yet, very few studies investigated the behaviour of EEG arrhythmic activity. Specifically, in a study of the human ECoG, the PSD showed a steeper decay across a broad frequency range in the four patients under propofol anesthesia, as compared to the one awake patient (Fig. 2 in Freeman et al., 2000) (Freeman et al., 2000). Furthermore, a bolus injection of propofol resulted in temporary

widespread decreases of the spectral exponent of the ECoG in macaques, with a time of onset and recovery time consistent with the loss and recovery of consciousness (Gao et al., 2017). Consistently, tiagabanine, an anesthetic with similar mechanism of action (GABA-a potentiation), increased the spectral exponent in human ECoG over a broad frequency range (5–100 Hz) (Muthukumaraswamy and Liley, 2018). Thus, propofol-induced large inhibition—mediated by GABA-A potentiation (Brown et al., 2011; Franks, 2008)—results in activity dampening (Solovey et al., 2015; Tagliazucchi et al., 2016) and in a steeper PSD decay—as indexed by a more negative spectral exponent (Gao et al., 2017).

4.4. Spectral exponent and mechanisms of action: xenon

Similarly to propofol, xenon yielded an overall slowing of the EEG across the 1–40 Hz range, as reflected by a decreased spectral exponent in the broad-band, as well as in the low and high frequency bands. This is consistent with previous literature, where xenon decreased the 95% spectral edge frequency (Goto et al., 2000; Laitio et al., 2008)—indexing an overall slowing of EEG activity—and largely increased low-frequency activity, in the delta and theta range (Laitio et al., 2008). Furthermore, xenon induced changes in the PSD that became progressively smaller as the frequency band increased from delta to beta—as expected when the overall PSD background becomes steeper (Laitio et al., 2008).

Contrarily to most anesthetics, xenon has little or no effect on GABA-A receptors (Franks et al., 1998). One of the proposed mechanisms of action of xenon is the potent non-competitive inhibition of N-methyl-D-aspartate (NMDA) receptors (Franks et al., 1998). Paradoxically, the antagonism of xenon on NMDA receptors may lead to over-excitation of cerebral wakefulness-promoting neurons—as indexed by increased norepinephrine and acetylcholine release—and thereby to loss of consciousness (Hirota, 2006).

Such over-excitation may seem at odd with the observed steepening of the PSD, according to previous hypothesis and simulation (Gao et al., 2017). However, this contradiction is only apparent. In this simulation (Gao et al., 2017), lowering the E/I ratio (from 1:2 to 1:6) towards deep inhibition resulted in a steeper PSD. Yet, in another simulation (Lombardi et al., 2017), a steeper PSD resulted from increasing the E/I ratio (from ~1:0.4 to 1:0) towards deep excitation. The latter situation seems more appropriate for xenon anesthesia. Future modelling studies should try to integrate these findings, by covering a wide range of E/I and verifying whether indeed the spectral exponent decreases in either states of deep inhibition and excitation.

Besides its antagonizing action on NMDA receptors, xenon acts primarily on two-pore-domain K+ (2 PK+) channels, strongly potentiating 2 PK+ conductance (Franks, 2008). Hence, xenon reduces the influence of excitatory currents (neuronal disfacilitation) thus possibly engendering a state of neuronal bistability (Timofeev et al., 2001). Neuronal bistability reflects an intrinsic propensity of cortical neurons to fall into silent hyperpolarized OFF-periods, which result in high-amplitude EEG slow-waves, both spontaneous and evoked by perturbations (Sarasso et al., 2015; Pigorini et al., 2015). Neuronal bistability has been thoroughly assessed in the realm of sleep physiology across different species and models. In this respect, *in silico*, *in vitro* as well as *in vivo* animal models suggests that neuronal bistability, and the ensuing activity dampening, may be due to adaptation mechanisms, such as neuronal disfacilitation (Compte, 2003; Sanchez-Vives and McCormick, 2000) as well as active inhibition (Funk et al., 2017; Zucca et al., 2017).

Altogether, neuronal bistability—mediated by 2 PK+ agonism—alone or in combination with increased excitation—mediated by NMDA receptor antagonism—may explain the prominent slowing of the EEG across the 1–40 Hz range and the steeper decay of the PSD during xenon.

4.5. Spectral exponent and mechanisms of action: ketamine

During ketamine, the spectral exponent β decreased slightly over the broad-band and, more pronouncedly, over the low-band, in all but one subject. This pattern is consistent with increased low-frequency power in the delta and theta band (Vlisides et al., 2017; Akeju et al., 2016; Wang et al., 2017). However, the broad-band spectral exponent across participants during ketamine was found widely overlapping with that of wakefulness (Fig. 4A). This is consistent with the preservation of conscious experience, despite profound unresponsiveness induced by the drug.

Moreover, in contrast to the other conditions (wakefulness, xenon- and propofol-anesthesia), during ketamine the PSD changed differently in the two portions of the spectrum. Specifically, while the PSD steepened in the low-band in all but one subject, the PSD markedly flattened in the high-band in all subjects (Fig. 4B). A remarkably similar shape of the PSD background in the two bands can be observed in previous EEG studies of ketamine anesthesia (Vlisides et al., 2017; Akeju et al., 2016; Maksimow et al., 2006). In addition, ketamine, even at subanesthetic doses (i.e. behavioural responsiveness maintained), differently affected two portions of the MEG spectrum (Muthukumaraswamy and Liley, 2018) in a similar fashion to that observed here.

It is conceivable that these changes in the shape of the PSD background can reflect the underlying mechanism of action of ketamine. Indeed ketamine acts primarily by binding to N-methyl-D-aspartate (NMDA) receptors, more effectively on interneurons than on pyramidal neurons (Purdon et al., 2015; Akeju et al., 2016). This results in down-regulation of the inhibitory tone, and thereby in higher excitability of pyramidal neurons, potentially explaining shallower slope and larger power in the high-frequency band. This is furthermore consistent with ketamine-induced increase of cerebral glucose consumption and blood flow (Langsjo et al., 2004; Långsjö et al., 2005). Regarding the lower end of the spectrum, animal studies (Miyasaka and Domino, 1968; Kayama and Iwama, 1972; Kiss et al., 2011; Zhang et al., 2012) suggest that the thalamus may play an essential role in the generation of low-frequency activity observed during ketamine. Specifically, NMDA-blockade mediated thalamic bursting may induce both theta and sporadic delta rhythms recorded with scalp EEG (Sarasso et al., 2015; Akeju et al., 2016). This may explain our observation of consistent, albeit non-significant, low-frequency steepening during ketamine anesthesia.

4.6. Ketamine temporal diversity: high-frequency arrhythmic activity

A flatter decay of the PSD indexes a reduction in temporal autocorrelations (He, 2014). Therefore, a near-flat decay of the PSD over the 20–40 Hz during ketamine anesthesia is consistent with the observation of increased temporal diversity of MEG signals during ketamine sedation (Schartner et al., 2017) and EEG signals during ketamine anesthesia (Wang et al., 2017). In these studies, temporal diversity was estimated with information-theoretic measures that rely upon binarization of the signal, according to the crossings around the mean/median of short epochs. Because high-frequency activity has an inherent high chance of crossing the mean/median, we reason that the observed higher signal diversity due to ketamine action in both studies is primarily due to the arrhythmic crossings of high-frequency activity. Conversely, in propofol, a steeper decay of the PSD could be interpreted as increased temporal autocorrelations (i.e. redundancy) (He, 2014), which is consistent with decreased randomness of EEG signals during propofol anesthesia (Wang et al., 2017). Conceivably, the same more ordered behaviour is to be expected for xenon anesthesia, despite no studies could be found up to date.

4.7. A steeper broad-band spectral exponent discriminate unconsciousness from consciousness

We have shown that the spectral exponent distinguished the 'No report' conditions (propofol and xenon anesthesia) from the 'Conscious report' conditions (wakefulness, ketamine anesthesia) in all cases and irrespectively of inter-individual differences in the spectral exponent.

This is valuable, since conscious experiences are often not reliably detected by common proprietary EEG-based anesthesia monitors (Russell, 2006; Samuelsson et al., 2008; Schneider et al., 2002). In the 'Conscious report' conditions, across wakefulness and ketamine anesthesia, the broad-band spectral exponent assumed values ~ -1 (β, mean [range]: −1.14 [-1.75, −0.74]). This finding is consistent with previous EEG (Dehghani et al., 2010; Pereda et al., 1998; Šušmáková, 2006) and MEG observations during wakefulness and ketamine sedation (Novikov et al., 1997; Muthukumaraswamy and Liley, 2018) as well as with MEG observations during the psychedelic drug LSD (Muthukumaraswamy and Liley, 2018). In contrast, in the 'No report' conditions (xenon and propofol anesthesia), the PSD showed a steeper decay across a broad band of frequencies (1–40 Hz). A steep PSD in the 'No report' condition was indexed by a large and negative spectral exponent, $\beta < 2$ (Fig. 4A). This is consistent with a slowing of the EEG and a redistribution of spectral power towards lower frequencies, typically observed in general anesthesia (Brown et al., 2010; Murphy et al., 2011; Laitio et al., 2008; Tonner and Bein, 2006).

4.8. Convergent validity: correlation with the perturbational complexity index

Finally, our results showed robust positive correlation between the spectral exponent of spontaneous activity and the Perturbational Complexity Index (PCI), obtained contextually over the same individuals (Sarasso et al., 2015). PCI is an empirical measure for the spatiotemporal EEG dynamics evoked by TMS, aimed at quantifying the joint presence of integration and differentiation (Casali et al., 2013), a fundamental requirement for the emergence of consciousness (Tononi and Edelman, 1998).

As discussed above, the spectral exponent has a tight relationship to the excitation and inhibition balance—as also supported by empirical and modelling evidence (Gao et al., 2017; Lombardi et al., 2017). The neural mechanisms balancing excitation and inhibition tightly regulate the proximity to a critical transition between activity propagation and extinction (Poil et al., 2012; Hellyer et al., 2016). Self-sustaining neural dynamics poised near criticality maximize the joint presence of integration and differentiation (Tagliazucchi, 2017). It is therefore compelling that both the spectral exponent and PCI peaked for states where excitation approximately balances inhibition—wakefulness and ketamine anesthesia—and were the lowest for states where the balance is disrupted—propofol and xenon anesthesia. This behaviour suggests a potential link between the spectral exponent and critical dynamics.

4.9. Scaling properties in different frequency bands

In the current study, we considered the overall decay of the background of the PSD over the 1–40 Hz range, thus encompassing all classic frequency bands of the EEG. The PSD decay was even more accurately described when considering the scaling properties of two adjacent subbands (1–20 Hz, 20–40 Hz), due to a bend or 'knee' at ~20 Hz. A singular scaling regime should be observed for at least two-orders of magnitude for both x and y axis, in order to have the statistical support to declare that a genuine power-law relationship exists (Stumpf and Porter, 2012). A power-law distribution is a classical signature of criticality (Bak et al., 1987). Recently, the framework has been extended to account for different scaling regimes in the power spectrum. For instance, one study introduced a dissipation factor to an activation/deactivation process, resulting in a bend or 'knee' in the PSD shape (De Los Rios and Zhang, 1999). Another study observed different scaling regions in the PSD of ECoG activity resulting from a slow/distributed and a fast/local mode of balanced activity propagation, as modelled by neural networks with recurrent random connectivity (Chaudhuri et al., 2018). A more realistic, physiologically constrained, corticothalamic model of the EEG was able to reproduce the sleep-related steepening of the 1/f-like decay in the low frequencies, and attributed the PSD 'knee' at ~20 Hz—as well as the steeper decay at higher frequencies—to the low-pass filtering properties of the dendrites (Robinson et al., 2001, 2011). Consistently, we here observed a steeper decay of the PSD in the high-frequencies during wakefulness as well as during xenon and propofol. Conversely, ketamine produced a remarkable flattening in the high-frequencies, independently from the low-frequencies (Vlisides et al., 2017; Akeju et al., 2016; Maksimow et al., 2006). A flatter PSD slope in high-frequencies encompassing the gamma range, as compared to the slope in the low frequencies, has been previously observed also in the human LFP (Freeman and Zhai, 2009). This upward deflection above a 'knee' frequency (around ~20 Hz) has been modelled by adding to the 1/f-like signal a flat-spectrum signal—proposed to represent the aggregate spiking activity of local neuronal populations (Gao, 2016).

We warrant caution in generalizing the results to different recording set-ups and experimental models, where different scaling regimes could be observed. Comparisons across studies should be carefully undertaken, also due the different frequency ranges under scrutiny. For instance, due to the problem of fitting a power-law where oscillations are present, the empirical studies in (Gao et al., 2017) select a range of frequencies between 30 and 70 Hz. However, the computational model presented in (Gao et al., 2017) suggests a tighter relationship between the E/I and the PSD slope over the 10–30 Hz and the 20–40 Hz range. Indeed, several studies observed that sleep depth decreased the spectral exponent, estimated from low to high frequencies (He et al., 2010; Freeman and Zhai, 2009; Pereda et al., 1998; Freeman, 2006; Šušmáková, 2006). However, the EEG spectral scaling exponent of infra-slow frequencies decreased with sleep depth (Lei et al., 2014)—yielding a shallower decay of the PSD over 0.06–3 Hz—thus revealing an opposite pattern to that typically observed at higher frequencies. Future studies should investigate the relationship between scaling exponents across a wide frequency range, while devising solid strategies to minimize the influence of physiological-, movement- and apparatus-induced artifacts (see Supplementary Material, section 7, for a detailed discussion on the potential contamination from ocular and muscular artifacts).

4.10. Future directions: intraoperative awareness, dreams and disorders of consciousness

PCI has shown to be a reliable marker for the presence of consciousness in brain-injured patients with disorders of consciousness (Casali et al., 2013; Casarotto et al., 2016). Given the robust positive correlation between PCI and the spectral exponent observed here, future work should test the ability of the spectral exponent in highlighting the presence of -and the recovery of-consciousness in brain-injured unresponsive patients. Concerning pharmacological manipulations, such as those here investigated, it would be also interesting to assess changes in the spectral exponent during the transition to unconsciousness. Along these lines, studies employing time-resolved EEG measures, such as the Direct Transfer Function, have shown the potential to track the transition from/to unconsciousness induced by anesthetic agents (Juel et al., 2018). Similarly, the spectral exponent can also be computed in a time-resolved fashion (Supplementary Material, section 8; Supplementary Figs. 8 and 9), thus showing the potential for real time monitoring of anesthesia-induced unconsciousness. Indeed, in this context, careful experimental settings should be designed in the attempt to systematically disentangle concentration-specific effects from proper changes in the level of consciousness (Radek et al., 2018; Scheinin et al., 2018b). Furthermore, it is expected that the spectral exponent should also be sensitive to the physiological fluctuations of the state of consciousness occurring during natural sleep, both across (Fagioli et al., 1989) as well as within specific sleep stages (Siclari et al., 2017).

In conclusion, the spectral exponent has proven across three different anesthetics to be a very promising feature, with both practical and theoretical implications, to index the presence of consciousness beyond sheer unresponsiveness.

Acknowledgments

Thanks to all the volunteers who made this work possible. Thanks to dr. Ezequiel Mikulan, dr. Anna Cattani and dr. Thierry Nieus for precious comments during the revision process. Thanks to the Liege department of anesthesia. This research has received funding from the Horizon 2020 Framework Programme for Research and Innovation under the Specific Grant Agreement No. 720270 (Human Brain Project SGA1) and No. 785907 (Human Brain Project SGA2), European Union (to M.M. and M.R.) and by the grant H2020, FETOPEN 2014-2015-RIA n. 686764 "Luminous", European Union (to M.M.). The study has also been partially funded by the grant "Sinergia" CRSII3_160803/1 of the Swiss National Science Foundation, Switzerland (to M.M.) and by the James S. McDonnell Foundation Scholar Award 2013, USA (to M.M.). and by the James S. McDonnell Foundation, Collaborative Activity Award 2013, USA (to S.L.).

The study has been partially funded by the grant "Giovani Ricercatori" GR-2011-02352031 of the Italian Ministry of Health, Italy (to M.R., M.A.C. and S.S.). The study was also supported by: the Belgian National Funds for Scientific Research (FRS-FNRS), Belgium (to S.L. and O.G.); the University and University Hospital of Liège, Belgium (to S.L. and O.G.); the Mind Science Foundation (to S.L.); the IAP research network P7/06 of the Belgian Government (Belgian Science Policy), Belgium (to S.L.); the European Commission, European Union (to S.L.); the Public Utility Foundation 'Université Européenne du Travail', Belgium (to S.L.); the "Fondazione Europea di Ricerca Biomedica", Italy (to S.L.) and the Bial Foundation (to S.L. and O.G.).

Appendix A. Supplementary data

Supplementary data to this article can be found online at https://doi.org/10.1016/j.neuroimage.2019.01.024.

Declarations of interest

None.

References

Akeju, O., Song, A.H., Hamilos, A.E., Pavone, K.J., Flores, F.J., Brown, E.N., et al., 2016. Electroencephalogram signatures of ketamine-induced unconsciousness. Clin Neurophysiol. Elsevier 127, 2414–2422. https://doi.org/10.1016/j.clinph.2016.03.005.

Bak, P., Tang, C., Wiesenfeld, K., 1987. Self-organized criticality: an explanation of the 1/f noise. Phys. Rev. Lett. 59, 381–384. https://doi.org/10.1103/PhysRevLett.59.381.

Bédard, C., Kröger, H., Destexhe, A., 2006. Does the 1/f frequency scaling of brain signals reflect self-organized critical states? Phys Rev Lett. Am. Phys. Soc. 97, 118102. https://doi.org/10.1103/PhysRevLett.97.118102.

Bowdle, T.A., Radant, A.D., Cowley, D.S., Kharasch, E.D., Strassman, R.J., Roy-Byrne, P.P., 1998. Psychedelic Effects of Ketamine in Healthy Volunteers: Relationship to Steady-State Plasma Concentrations, vol. 88. Lippincott Williams and Wilkins, Anesthesiology, pp. 82–88. https://doi.org/10.1097/00000542-199801000-00015.

Brown, E.N., Lydic, R., Schiff, N.D., 2010. General anesthesia, sleep, and coma. N. Engl. J. Med. 363, 2638–2650. https://doi.org/10.1056/NEJMra0808281.

Brown, E.N., Purdon, P.L., Van Dort, C.J., 2011. General anesthesia and altered states of arousal: a systems neuroscience analysis. Annu. Rev. Neurosci. 34, 601–628. https://doi.org/10.1146/annurev-neuro-060909-153200.

Buzsáki, G., Mizuseki, K., 2014. The log-dynamic brain: how skewed distributions affect network operations. Nat Rev Neurosci. Nature Publishing Group 15, 264–278. https://doi.org/10.1038/nrn3687.

Cantero, J.L., Atienza, M., Salas, R.M., 2002. Human alpha oscillations in wakefulness, drowsiness period, and REM sleep: different electroencephalographic phenomena within the alpha band. Neurophysiol. Clin. 32, 54–71. https://doi.org/10.1016/S0987-7053(01)00289-1.

Carhart-Harris, R.L., Leech, R., Hellyer, P.J., Shanahan, M., Feilding, A., Tagliazucchi, E., et al., 2014. The entropic brain: a theory of conscious states informed by neuroimaging research with psychedelic drugs. Front Hum Neurosci. Frontiers 8, 20. https://doi.org/10.3389/fnhum.2014.00020.

Casali, A.G., Gosseries, O., Rosanova, M., Boly, M., Sarasso, S., Casali, K.R., et al., 2013. A theoretically based index of consciousness independent of sensory processing and behavior. Sci. Transl. Med. 5 https://doi.org/10.1126/scitranslmed.3006294, 198ra105-198ra105.

Casarotto, S., Comanducci, A., Rosanova, M., Sarasso, S., Fecchio, M., Napolitani, M., et al., 2016. Stratification of unresponsive patients by an independently validated index of brain complexity. Ann. Neurol. 80, 718–729. https://doi.org/10.1002/ana.24779.

Chaudhuri, R., He, B.J., Wang, X.J., 2018. Random Recurrent Networks Near Criticality Capture the Broadband Power Distribution of Human ECoG Dynamics. Cereb Cortex, vol. 28. Oxford University Press, pp. 3610–3622. https://doi.org/10.1093/cercor/bhx233.

Chennu, S., Finoia, P., Kamau, E., Allanson, J., Williams, G.B., Monti, M.M., et al., 2014. Spectral signatures of reorganised brain networks in disorders of consciousness. PLoS Comput. Biol. 10 https://doi.org/10.1371/journal.pcbi.1003887.

Ciuciu, P., Varoquaux, G., Abry, P., Sadaghiani, S., Kleinschmidt, A., 2012. Scale-free and multifractal time dynamics of fMRI signals during rest and task. Front Physiol. Frontiers 3, 186. https://doi.org/10.3389/fphys.2012.00186.

Coleman, M.R., Menon, D.K., Fryer, T.D., Pickard, J.D., 2005. Neurometabolic coupling in the vegetative and minimally conscious states: preliminary findings. J. Neurol. Neurosurg. Psychiatry 76, 432–434. https://doi.org/10.1136/jnnp.2004.045930. BMJ Publishing Group Ltd.

Compte, A., 2003. Cellular and network mechanisms of slow oscillatory activity (<1 Hz) and wave propagations in a cortical network model. J. Neurophysiol. 89, 2707–2725. https://doi.org/10.1152/jn.00845.2002.

De Gennaro, L., Ferrara, M., Bertini, M., 2001. The boundary between wakefulness and sleep: quantitative electroencephalographic changes during the sleep onset period. Neuroscience 107, 1–11. https://doi.org/10.1016/S0306-4522(01)00309-8.

De Los Rios, P., Zhang, Y.-C., 1999. Universal 1/f noise from dissipative self-organized criticality models. Phys Rev Lett. Am. Phys. Soc. 82, 472–475. https://doi.org/10.1103/PhysRevLett.82.472.

Dehghani, N., Bédard, C., Cash, S.S., Halgren, E., Destexhe, A., 2010. Comparative power spectral analysis of simultaneous elecroencephalographic and magnetoencephalographic recordings in humans suggests non-resistive extracellular media. J. Comput. Neurosci. Springer US 29, 405–421. https://doi.org/10.1007/s10827-010-0263-2.

Destexhe, A., Rudolph, M., Paré, D., 2003. The high-conductance state of neocortical neurons in vivo. Nat Rev Neurosci. Nature Publishing Group 4, 739–751. https://doi.org/10.1038/nrn1198.

DiNuzzo, M., Mangia, S., Maraviglia, B., Giove, F., 2014. Physiological bases of the K+ and the glutamate/GABA hypotheses of epilepsy. Epilepsy Res. NIH Public Access 108, 995–1012. https://doi.org/10.1016/j.eplepsyres.2014.04.001.

Estraneo, A., Loreto, V., Guarino, I., Boemia, V., Paone, G., Moretta, P., et al., 2016. Standard EEG in diagnostic process of prolonged disorders of consciousness. Clin Neurophysiol. Elsevier 127, 2379–2385. https://doi.org/10.1016/J.CLINPH.2016.03.021.

Fagioli, I., Cipolli, C., Tuozzi, G., 1989. Accessing previous mental sleep experience in REM and NREM sleep. Biol. Psychol. 29, 27–38. Available: http://www.ncbi.nlm.nih.gov/pubmed/2590707.

Finelli, L.A., Baumann, H., Borbély, A.A., Achermann, P., 2000. Dual electroencephalogram markers of human sleep homeostasis: correlation between theta activity in waking and slow-wave activity in sleep. Neuroscience. Pergamon 101, 523–529. https://doi.org/10.1016/S0306-4522(00)00409-7.

Fiset, P., Daloze, T., Plourde, G., Meuret, P., Bonhomme, V., Hajj-ali, N., et al., 1999. Brain mechanisms of propofol-induced loss of consciousness in humans: a positron emission tomographic study. J. Neurosci. 19, 5506–5513. https://doi.org/10.1523/JNEUROSCI.19-13-05506.1999.

Franks, N.P., 2008. General anaesthesia: from molecular targets to neuronal pathways of sleep and arousal [Internet]. Nat. Rev. Neurosci. 370–386. https://doi.org/10.1038/nrn2372.

Franks, N.P., Dickinson, R., De Sousa, S.L.M., Hall, A.C., Lieb, W.R., 1998. How does xenon produce anaesthesia? [Internet]. Nature 324. https://doi.org/10.1038/24525.

Freeman, W.J., 2006. Origin, structure, and role of background EEG activity. Part 4: neural frame simulation. Clin. Neurophysiol. 117, 572–589. https://doi.org/10.1016/j.clinph.2005.10.025.

Freeman, W.J., Zhai, J., 2009. Simulated Power Spectral Density (PSD) of Background Electrocorticogram (ECoG). Cogn Neurodyn, vol. 3. Springer Netherlands, pp. 97–103. https://doi.org/10.1007/s11571-008-9064-y.

Freeman, W.J., Rogers, L.J., Holmes, M.D., Silbergeld, D.L., 2000. Spatial spectral analysis of human electrocorticograms including the alpha and gamma bands. J. Neurosci. Methods 95, 111–121. https://doi.org/10.1016/S0165-0270(99)00160-0. Elsevier.

Funk, C.M., Peelman, K., Bellesi, M., Marshall, W., Cirelli, C., Tononi, G., 2017. Role of somatostatin-positive cortical interneurons in the generation of sleep slow waves. J. Neurosci. 1303–1317. https://doi.org/10.1523/JNEUROSCI.1303-17.2017.

Gao, R., 2016. Interpreting the electrophysiological power spectrum. J. Neurophysiol. 115, 628–630. https://doi.org/10.1152/jn.00722.2015.

Gao, R., Peterson, E.J., Voytek, B., 2017. Inferring Synaptic Excitation/inhibition Balance from Field Potentials. Neuroimage, vol. 158. Academic Press, pp. 70–78. https://doi.org/10.1016/J.NEUROIMAGE.2017.06.078.

Giacino, J.T., Kalmar, K., Whyte, J., 2004. The JFK coma recovery scale-revised: measurement characteristics and diagnostic utility. Arch. Phys. Med. Rehabil. 85, 2020–2029. https://doi.org/10.1016/J.APMR.2004.02.033. W.B. Saunders.

Goto, T., Nakata, Y., Saito, H., Ishiguro, Y., Niimi, Y., Suwa, K., et al., 2000. Bispectral Analysis of the Electroencephalogram Does Not Predict Responsiveness to Verbal Command in Patients Emerging from Xenon Anaesthesia†. Br J Anaesth, vol. 85. Oxford University Press, pp. 359–363. https://doi.org/10.1093/bja/85.3.359.

Gouzoulis-Mayfrank, E., Heekeren, K., Neukirch, A., Stoll, M., Stock, C., Obradovic, M., et al., 2005. Psychological effects of (S)-ketamine and N,N-dimethyltryptamine (DMT): a double-blind, cross-over study in healthy volunteers. Pharmacopsychiatry 38, 301–311. https://doi.org/10.1055/s-2005-916185.

Hahn, G., Ponce-Alvarez, A., Monier, C., Benvenuti, G., Kumar, A., dé ric Chavane, F., et al., 2017. Spontaneous cortical activity is transiently poised close to criticality. Hilgetag CC. PLOS Comput Biol. Public Library of Science 13, e1005543. https://doi.org/10.1371/journal.pcbi.1005543.

He, B.J., 2011. Scale-free properties of the functional magnetic resonance imaging signal during rest and task. J Neurosci. Society for Neuroscience 31, 13786–13795. https://doi.org/10.1523/JNEUROSCI.2111-11.2011.

He, B.J., 2014. Scale-free brain activity: past, present, and future. Trends Cognit. Sci. 18, 480–487. https://doi.org/10.1016/j.tics.2014.04.003.

He, B.J., Zempel, J.M., Snyder, A.Z., Raichle, M.E., 2010. The temporal structures and functional significance of scale-free brain activity. Neuron. Elsevier 66, 353–369. https://doi.org/10.1016/j.neuron.2010.04.020.

Hellyer, P.J., Jachs, B., Clopath, C., Leech, R., 2016. Local inhibitory plasticity tunes macroscopic brain dynamics and allows the emergence of functional brain networks. Neuroimage 124, 85–95. https://doi.org/10.1016/j.neuroimage.2015.08.069.

Hirota, K., 2006. Special cases: ketamine, nitrous oxide and xenon. Best Pract Res Clin Anaesthesiol. Baillière Tindall 20, 69–79. https://doi.org/10.1016/J.BPA.2005.08.014.

Hobson, J a, Pace-Schott, E.F., Stickgold, R., 2000. Dreaming and the brain: toward a cognitive neuroscience of conscious states. Behav. Brain Sci. 23, 793–842 discussion 904-1121. Available: http://www.ncbi.nlm.nih.gov/pubmed/11515143.

Hung, C.-S., Sarasso, S., Ferrarelli, F., Riedner, B., Ghilardi, M.F., Cirelli, C., et al., 2013. Local experience-dependent changes in the wake EEG after prolonged wakefulness. Sleep 36, 59–72. https://doi.org/10.5665/sleep.2302.

Hwa, R.C., Ferree, T.C., 2002. Scaling properties of fluctuations in the human electroencephalogram. Phys Rev E - Stat Physics, Plasmas, Fluids, Relat Interdiscip Top. American Physical Society 66, 021901. https://doi.org/10.1103/PhysRevE.66.021901.

Jones, C., 1979. Glasgow coma scale. Am. J. Nurs. 79, 1551. https://doi.org/10.2307/3424679.

Juel, B.E., Romundstad, L., Kolstad, F., Storm, J.F., Larsson, P.G., 2018. Distinguishing anesthetized from awake state in patients: a new approach using one second segments of raw EEG. Front Hum Neurosci. Frontiers 12, 40. https://doi.org/10.3389/fnhum.2018.00040.

Kantelhardt, J.W., Tismer, S., Gans, F., Schumann, A.Y., Penzel, T., 2015. Scaling behavior of EEG amplitude and frequency time series across sleep stages. EPL (Europhysics Lett. 112, 18001. https://doi.org/10.1209/0295-5075/112/18001.

Kayama, Y., Iwama, K., 1972. The EEG, evoked potentials, and single-unit activity during ketamine anesthesia in cats. Anesthesiology 36, 316–328. Available: https://insights.ovid.com/anesthesiology/anet/1972/04/000/eeg-evoked-potentials-single-unit-activity-during/4/00000542.

Kiefer, R.T., Rohr, P., Ploppa, A., Dieterich, H.J., Grothusen, J., Koffler, S., et al., 2008. Efficacy of Ketamine in Anesthetic Dosage for the Treatment of Refractory Complex Regional Pain Syndrome: an Open-Label Phase II Study. Pain Med, vol. 9. Oxford University Press, pp. 1173–1201. https://doi.org/10.1111/j.1526-4637.2007.00402.x.

Kiss, T., Hoffmann, W.E., Scott, L., Kawabe, T.T., Milici, A.J., Nilsen, E.A., et al., 2011. Role of thalamic projection in NMDA receptor-induced disruption of cortical slow oscillation and short-term plasticity. Front Psychiatry. Frontiers 2, 14. https://doi.org/10.3389/fpsyt.2011.00014.

Klimesch, W., Sauseng, P., Hanslmayr, S., 2007. EEG alpha oscillations: the inhibition-timing hypothesis. Brain Res. Rev. 53, 63–88. https://doi.org/10.1016/j.brainresrev.2006.06.003.

Koch, C., Massimini, M., Boly, M., Tononi, G., 2016. Neural correlates of consciousness: progress and problems. Nat. Rev. Neurosci. 17 https://doi.org/10.1038/nrn.2016.61, 395–395.

Laitio, R.M., Kaskinoro, K., Särkelä, M.O.K., Kaisti, K.K., Salmi, E., Maksimow, A., et al., 2008. Bispectral index, entropy, and quantitative electroencephalogram during single-agent xenon anesthesia. Anesthesiol. Am. Soc. Anesthesiol. 108, 63–70. https://doi.org/10.1097/01.anes.0000296106.52472.a6.

Langsjo, J.W., Salmi, E., Kaisti, K.K., Aalto, S., Hinkka, S., Aantaa, R., et al., 2004. Effects of subanesthetic ketamine on regional cerebral glucose metabolism in humans. Anesthesiology 100, 1065–1071. Available: http://anesthesiology.pubs.asahq.org/article.aspx?articleid=1943736.

Långsjö, J.W., Maksimow, A., Salmi, E., Kaisti, K., Aalto, S., Oikonen, V., et al., 2005. S-ketamine anesthesia increases cerebral blood flow in excess of the metabolic needs in humans. Anesthesiology 103, 258–268. https://doi.org/10.1097/00000542-200508000-00008.

Lechinger, J., Bothe, K., Pichler, G., Michitsch, G., Donis, J., Klimesch, W., et al., 2013. CRS-R score in disorders of consciousness is strongly related to spectral EEG at rest. J. Neurol. 260, 2348–2356. https://doi.org/10.1007/s00415-013-6982-3.

Lee, U., Ku, S., Noh, G., Baek, S., Choi, B., Mashour, G a, 2013. Disruption of frontal-parietal communication by ketamine, propofol, and sevoflurane. Anesthesiology 118, 1264–1275. https://doi.org/10.1097/ALN.0b013e31829103f5.

Leemburg, S., Gao, B., Cam, E., Sarnthein, J., Bassetti, C.L., 2018. Power spectrum slope and motor function recovery after focal cerebral ischemia in the rat. bioRxiv. Cold Spring Harbor Laboratory 242388. https://doi.org/10.1101/242388.

Lei, X., Wang, Y., Yuan, H., Chen, A., 2014. Brain scale-free properties in awake rest and NREM sleep: a simultaneous EEG/fMRI study. Brain Topogr. 28, 292–304. https://doi.org/10.1007/s10548-014-0399-x.

Lombardi, F., Herrmann, H.J., de Arcangelis, L., 2017. Balance of excitation and inhibition determines 1/f power spectrum in neuronal networks. Chaos. An Interdiscip. J. Nonlinear Sci. 27, 047402 https://doi.org/10.1063/1.4979043. AIP Publishing LLC.

Maksimow, A., Särkelä, M., Långsjö, J.W., Salmi, E., Kaisti, K.K., Yli-Hankala, A., et al., 2006. Increase in high frequency EEG activity explains the poor performance of EEG spectral entropy monitor during S-ketamine anesthesia. Clin Neurophysiol. Elsevier 117, 1660–1668. https://doi.org/10.1016/J.CLINPH.2006.05.011.

Manning, J.R., Jacobs, J., Fried, I., Kahana, M.J., 2009. Broadband shifts in local field potential power spectra are correlated with single-neuron spiking in humans. J. Neurosci. Soc. Neurosci. 29, 13613–13620. https://doi.org/10.1523/JNEUROSCI.2041-09.2009.

Marsh, B., White, M., Morton, N., Kenny, G.N.C., 1991. Pharmacokinetic model diven infusion of propofol in children. Br. J. Anaesth. 67, 41–48. Available: https://academic.oup.com/bja/article-abstract/67/1/41/283883.

Meisel, C., Storch, A., Hallmeyer-Elgner, S., Bullmore, E., Gross, T., 2012. Failure of adaptive self-organized criticality during epileptic seizure attacks. PLoS Comput Biol. Public Library of Science 8, e1002312. https://doi.org/10.1371/journal.pcbi.1002312.

Meisel, C., Klaus, A., Vyazovskiy, V.V., Plenz, D., 2017. The Interplay between Long- and Short-Range Temporal Correlations Shapes Cortex Dynamics across Vigilance States. https://doi.org/10.1523/JNEUROSCI.0448-17.2017.

Merica, H., Blois, R., 1997. Relationship between the time courses of power in the frequency bands of human sleep EEG. In: Neurophysiol Clin Neurophysiol, vol. 27. Elsevier Masson, pp. 116–128. https://doi.org/10.1016/S0987-7053(97)85664-X.

Miller, K.J., Sorensen, L.B., Ojemann, J.G., Den Nijs, M., 2009. Power-law scaling in the brain surface electric potential. In: Sporns, O. (Ed.), PLoS Comput Biol. Society for Neuroscience 5, e1000609. https://doi.org/10.1371/journal.pcbi.1000609.

Miller, A.C., Jamin, C.T., Elamin, E.M., 2011. Continuous Intravenous Infusion of Ketamine for Maintenance Sedation [Internet]. Minerva Anestesiologica, pp. 812–820. Available: https://emcrit.org/wp-content/uploads/2012/11/cont-infusion-ketamine.pdf.

Milstein, J., Mormann, F., Fried, I., Koch, C., 2009. In: de la Prida, L.M. (Ed.), Neuronal Shot Noise and Brownian 1/f2 Behavior in the Local Field Potential, vol. 4. Public Library of Science, p. e4338. https://doi.org/10.1371/journal.pone.0004338. PLoS One.

Miskovic, V., MacDonald, K.J., Rhodes, L.J., Cote, K.A., 2018. Changes in EEG Multiscale Entropy and Power-Law Frequency Scaling during the Human Sleep Cycle. Hum Brain Mapp. Wiley-Blackwell. https://doi.org/10.1002/hbm.24393.

Miyasaka, M., Domino, E.F., 1968. Neuronal mechanisms of ketamine-induced anesthesia. Int J Neuropharmacol. Pergamon 7, 557–573. https://doi.org/10.1016/0028-3908(68)90067-1.

Murphy, M., Bruno, M.-A., Riedner, B a, Boveroux, P., Noirhomme, Q., Landsness, E.C., et al., 2011. Propofol anesthesia and sleep: a high-density EEG study. Sleep 34, 283–91A. Available: http://www.pubmedcentral.nih.gov/articlerender.fcgi?artid=3041704&tool=pmcentrez&rendertype=abstract.

Muthukumaraswamy, S.D., Liley, D.T., 2018. 1/f Electrophysiological Spectra in Resting and Drug-Induced States Can Be Explained by the Dynamics of Multiple Oscillatory Relaxation Processes. Neuroimage, vol. 179. Academic Press, pp. 582–595. https://doi.org/10.1016/J.NEUROIMAGE.2018.06.068.

Novikov, E., Novikov, A., Shannahoff-Khalsa, D., Schwartz, B., Wright, J., 1997. Scale-similar activity in the brain. Phys Rev E - Stat Physics, Plasmas, Fluids, Relat Interdiscip Top. 56, R2387–R2389. https://doi.org/10.1103/PhysRevE.56.R2387.

Ogilvie, R.D., 2001. The process of falling asleep. Sleep Med. Rev. 5, 247–270. https://doi.org/10.1053/smrv.2001.0145.

Oken, B.S., Salinsky, M.C., Elsas, S.M., 2006. Vigilance, alertness, or sustained attention: physiological basis and measurement. Clin. Neurophysiol. 117, 1885–1901. https://doi.org/10.1016/j.clinph.2006.01.017.

Palva, S., Palva, J.M., 2018. Roles of brain criticality and multiscale oscillations in temporal predictions for sensorimotor processing. Trends Neurosci. Elsevier Current Trends 41, 729–743. https://doi.org/10.1016/J.TINS.2018.08.008.

Pearlmutter, B.A., Houghton, C.J., 2009. A new hypothesis for Sleep : tuning for criticality. Neural Comput. 21, 1622–1641. https://doi.org/10.1162/neco.2009.05-08-787.

Pereda, E., Gamundi, A., Rial, R., González, J., 1998. Non-linear behaviour of human EEG: fractal exponent versus correlation dimension in awake and sleep stages. Neurosci. Lett. 250, 91–94. https://doi.org/10.1016/S0304-3940(98)00435-2.

Pigorini, A., Sarasso, S., Proserpio, P., Szymanski, C., Arnulfo, G., Casarotto, S., et al., 2015. Bistability Breaks-Off Deterministic Responses to Intracortical Stimulation during Non-REM Sleep, vol. 112. Neuroimage. Academic Press, pp. 105–113. https://doi.org/10.1016/J.NEUROIMAGE.2015.02.056.

Poil, S.-S., Hardstone, R., Mansvelder, H.D., Linkenkaer-Hansen, K., 2012. Critical-state dynamics of avalanches and oscillations jointly emerge from balanced excitation/inhibition in neuronal networks. J. Neurosci. 32, 9817–9823. https://doi.org/10.1523/JNEUROSCI.5990-11.2012.

Preller, K.H., Vollenweider, F.X., 2018. Phenomenology, Structure, and Dynamic of Psychedelic States. Current Topics in Behavioral Neurosciences. Springer, Berlin, Heidelberg, pp. 221–256. https://doi.org/10.1007/7854_2016_459.

Priesemann, V., Valderrama, M., Wibral, M., Le Van Quyen, M., 2013. Neuronal avalanches differ from wakefulness to deep sleep–evidence from intracranial depth recordings in humans. In: Sporns, O. (Ed.), PLoS Comput Biol, vol. 9. Public Library of Science;, e1002985 https://doi.org/10.1371/journal.pcbi.1002985.

Priesemann, V., Wibral, M., Valderrama, M., Pröpper, R., Le Van Quyen, M., Geisel, T., et al., 2014. Spike avalanches in vivo suggest a driven, slightly subcritical brain state. Front. Syst. Neurosci. 8, 108. https://doi.org/10.3389/fnsys.2014.00108.

Pritchard, W.S., 1992. The brain in fractal time: 1/f-like power spectrum scaling of the human electroencephalogram. Int. J. Neurosci. 66, 119–129. https://doi.org/10.3109/00207459208999796.

Purdon, P.L., Sampson, A., Pavone, K.J., Brown, E.N., 2015. Clinical Electroencephalography for Anesthesiologists [Internet]. Anesthesiology. The American Society of Anesthesiologists, pp. 937–960. https://doi.org/10.1097/ALN.0000000000000841.

Radek, L., Kallionpää, R.E., Karvonen, M., Scheinin, A., Maksimow, A., Långsjö, J., et al., 1 Jul 2018. Dreaming and awareness during dexmedetomidine- and propofol-induced unresponsiveness. Br. J. Anaesth. 260–269. https://doi.org/10.1016/j.bja.2018.03.014. Elsevier.

Ramsay, M.A., Savege, T.M., Simpson, B.R., Goodwin, R., 1974. Controlled sedation with alphaxalone-alphadolone. Br. Med. J. 2, 656–659. Available: http://www.ncbi.nlm.nih.gov/pubmed/4835444.

Rex, S., Schaefer, W., Meyer, P.H., Rossaint, R., Boy, C., Setani, K., et al., 2006. Positron emission tomography study of regional cerebral metabolism during general anesthesia with xenon in humans. Anesthesiology 105, 936–943, 00000542-200611000-00014.

Robinson, P a, Rennie, C.J., Wright, J.J., Bahramali, H., Gordon, E., Rowe, D.L., 2001. Prediction of electroencephalographic spectra from neurophysiology. Phys. Rev. E - Stat. Nonlinear Soft Matter Phys. 63, 1–18. https://doi.org/10.1103/PhysRevE.63.021903.

Robinson, P a, Phillips, a JK., Fulcher, B.D., Puckeridge, M., Roberts, J a, 2011. Quantitative modelling of sleep dynamics. Philos. Trans. A Math. Phys. Eng. Sci. 369, 3840–3854. https://doi.org/10.1098/rsta.2011.0120.

Russell, I.F., 2006. The Narcotrend "Depth of Anaesthesia" Monitor Cannot Reliably Detect Consciousness during General Anaesthesia: an Investigation Using the Isolated Forearm Technique. Br J Anaesth, vol. 96. Oxford University Press, pp. 346–352. https://doi.org/10.1093/bja/ael017.

Samuelsson, P., Brudin, L., Sandin, R.H., 2008. BIS does not predict dreams reported after anaesthesia. Acta Anaesthesiol. Scand. 52, 810–814. https://doi.org/10.1111/j.1399-6576.2008.01633.x.

Sanchez-Vives, M.V., McCormick, D.A., 2000. Cellular and network mechanisms of rhytmic recurrent activity in neocortex. Nat. Neurosci. 3, 1027–1034. https://doi.org/10.1038/79848.

Sanders, R.D., Tononi, G., Laureys, S., Sleigh, J.W., 2012. Unresponsiveness ≠ unconsciousness. Anesthesiology. Am. Soc. Anesthesiol. 116, 946–959. https://doi.org/10.1097/ALN.0b013e318249d0a7.

Sarasso, S., Boly, M., Napolitani, M., Gosseries, O., Charland-Verville, V., Casarotto, S., et al., 2015. Consciousness and complexity during unresponsiveness induced by propofol, xenon, and ketamine. Curr Biol. Elsevier 25, 3099–3105. https://doi.org/10.1016/j.cub.2015.10.014.

Schartner, M.M., Carhart-Harris, R.L., Barrett, A.B., Seth, A.K., Muthukumaraswamy, S.D., 2017. Increased spontaneous MEG signal diversity for psychoactive doses of ketamine, LSD and psilocybin. Sci Rep. Nature Publishing Group 7, 46421. https://doi.org/10.1038/srep46421.

Scheinin, A., Kallionpää, R.E., Li, D., Kallioinen, M., Kaisti, K., Långsjö, J., et al., 2018. Differentiating drug-related and state-related effects of dexmedetomidine and propofol on the electroencephalogram. Anesthesiology 1. https://doi.org/10.1097/ALN.0000000000002192.

Scheinin, A., Kallionpää, R.E., Li, D., Kallioinen, M., Kaisti, K., Långsjö, J., et al., 2018. Differentiating drug-related and state-related effects of dexmedetomidine and propofol on the electroencephalogram. Anesthesiology 1. https://doi.org/10.1097/ALN.0000000000002192.

Schneider, G., Wagner, K., Reeker, W., Hänel, F., Werner, C., Kochs, E., 2002. Bispectral index (BIS) may not predict awareness reaction to intubation in surgical patients. J. Neurosurg. Anesthesiol. 14, 7–11. https://doi.org/10.1097/00008506-200201000-00002.

Scott, G., Fagerholm, E.D., Mutoh, H., Leech, R., Sharp, D.J., Shew, W.L., et al., 2014. Voltage imaging of waking mouse cortex reveals emergence of critical neuronal dynamics. J. Neurosci. Soc. Neurosci. 34, 16611–16620. https://doi.org/10.1523/JNEUROSCI.3474-14.2014.

Shen, Y., Olbrich, E., Achermann, P., Meier, P.F., 2003. Dimensional complexity and spectral properties of the human sleep EEG. Clin Neurophysiol. Elsevier 114, 199–209. https://doi.org/10.1016/S1388-2457(02)00338-3.

Siclari, F., Baird, B., Perogamvros, L., Bernardi, G., LaRocque, J.J., Riedner, B., et al., 2017. The neural correlates of dreaming. Nat Neurosci. NIH Public Access 20, 872–878. https://doi.org/10.1038/nn.4545.

Sitt, J.D., King, J.-R., El Karoui, I., Rohaut, B., Faugeras, F., Gramfort, A., et al., 2014. Large Scale Screening of Neural Signatures of Consciousness in Patients in a Vegetative or Minimally Conscious State, vol. 137. Oxford University Press, Brain, pp. 2258–2270. https://doi.org/10.1093/brain/awu141.

Solovey, G., Alonso, L.M., Yanagawa, T., Fujii, N., Magnasco, M.O., Cecchi, G.A., et al., 2015. Loss of consciousness is associated with stabilization of cortical activity. J. Neurosci. Soc. Neurosci. 35, 10866–10877. https://doi.org/10.1523/JNEUROSCI.4895-14.2015.

Steyn-Ross, M.L., Steyn-Ross, D a, Sleigh, J.W., 2004. Modelling general anaesthesia as a first-order phase transition in the cortex. Prog. Biophys. Mol. Biol. 85, 369–385. https://doi.org/10.1016/j.pbiomolbio.2004.02.001.

Stumpf, M.P.H.H., Porter, M a, 2012. Critical truths about power laws. Science 335, 665–666. https://doi.org/10.1126/science.1216142.

Šušmáková, K., 2006. Correlation dimension versus fractal exponent during sleep onset. Meas. Sci. Rev. 6, 58–62.

Tagliazucchi, E., 2017. The Signatures of Conscious Access and its Phenomenology Are Consistent with Large-Scale Brain Communication at Criticality. Conscious Cogn, vol. 55. Academic Press, pp. 136–147. https://doi.org/10.1016/j.concog.2017.08.008.

Tagliazucchi, E., von Wegner, F., Morzelewski, A., Brodbeck, V., Jahnke, K., Laufs, H., 2013. Breakdown of long-range temporal dependence in default mode and attention networks during deep sleep. Proc. Natl. Acad. Sci. U. S. A. 110, 15419–15424. https://doi.org/10.1073/pnas.1312848110.

Tagliazucchi, E., Chialvo, D.R., Siniatchkin, M., Amico, E., Brichant, J.-F., Bonhomme, V., et al., 2016. Large-scale signatures of unconsciousness are consistent with a departure from critical dynamics. J R Soc Interface. The Royal Society 13, 20151027. https://doi.org/10.1098/rsif.2015.1027.

Timofeev, I., Grenier, F., Steriade, M., 2001. Disfacilitation and active inhibition in the neocortex during the natural sleep-wake cycle: an intracellular study. Proc Natl Acad Sci. Nat. Acad. Sci. 98, 1924–1929. https://doi.org/10.1073/pnas.041430398.

Tonner, P.H., Bein, B., 2006. Classic Electroencephalographic Parameters: Median Frequency, Spectral Edge Frequency Etc. Best Practice and Research: Clinical Anaesthesiology, pp. 147–159. https://doi.org/10.1016/j.bpa.2005.08.008.

Tononi, G., Edelman, G.M., 1998. Consciousness and complexity. Science 282, 1846–1851. Available: http://www.ncbi.nlm.nih.gov/pubmed/22255149.

Vlisides, P.E., Bel-Bahar, T., Lee, U.C., Li, D., Kim, H., Janke, E., et al., 2017. Neurophysiologic correlates of ketamine sedation and anesthesia: a high-density electroencephalography study in healthy volunteers. Anesthesiology. Am. Soc. Anesthesiol. 127, 58–69. https://doi.org/10.1097/ALN.0000000000001671.

Wang, J., Noh, G.-J., Choi, B.-M., Ku, S.-W., Joo, P., Jung, W.-S., et al., 2017. Suppressed Neural Complexity during Ketamine- and Propofol-Induced Unconsciousness, vol. 653. Neurosci Lett. Elsevier, pp. 320–325. https://doi.org/10.1016/J.NEULET.2017.05.045.

Wen, H., Liu, Z., 2016. Separating fractal and oscillatory components in the power spectrum of neurophysiological signal. In: Brain Topogr, vol. 29. Springer US, pp. 13–26. https://doi.org/10.1007/s10548-015-0448-0.

Zhang, Y., Yoshida, T., Katz, D.B., Lisman, J.E., 2012. NMDAR antagonist action in thalamus imposes delta oscillations on the hippocampus. J. Neurophysiol. Am. Physiol. Soc. Bethesda, MD 107, 3181–3189. https://doi.org/10.1152/jn.00072.2012.

Zhou, D.W., Mowrey, D.D., Tang, P., Xu, Y., 2015. Percolation model of sensory transmission and loss of consciousness under general anesthesia. Phys. Rev. Lett. 115 https://doi.org/10.1103/PhysRevLett.115.108103.

Zucca, S., D'Urso, G., Pasquale, V., Vecchia, D., Pica, G., Bovetti, S., et al., 2017. An inhibitory gate for state transition in cortex. Elife 6. https://doi.org/10.7554/eLife.26177.